Energetic overturning flows, dynamic interocean exchanges, and ocean warming observed in the South Atlantic

María Paz Chidichimo, Renellys C. Perez, Sabrina Speich, Marion Kersalé, Janet Sprintall, Shenfu Dong, Tarron Lamont, Olga T. Sato, Teresa K. Chereskin, Rebecca Hummels, et al.

communications earth & environment

REVIEW ARTICLE

https://doi.org/10.1038/s43247-022-00644-x OPEN

Energetic overturning flows, dynamic interocean exchanges, and ocean warming observed in the South Atlantic

María Paz Chidichimo[1,2,3✉], Renellys C. Perez[4], Sabrina Speich[5], Marion Kersalé[6], Janet Sprintall[7], Shenfu Dong[4], Tarron Lamont[8,9,10], Olga T. Sato[11], Teresa K. Chereskin[7], Rebecca Hummels[12] & Claudia Schmid[4]

Since the inception of the international South Atlantic Meridional Overturning Circulation initiative in the 21st century, substantial advances have been made in observing and understanding the Southern Hemisphere component of the Atlantic Meridional Overturning Circulation (AMOC). Here we synthesize insights gained into overturning flows, interocean exchanges, and water mass distributions and pathways in the South Atlantic. The overturning circulation in the South Atlantic uniquely carries heat equatorward and exports freshwater poleward and consists of two strong overturning cells. Density and pressure gradients, winds, eddies, boundary currents, and interocean exchanges create an energetic circulation in the subtropical and tropical South Atlantic Ocean. The relative importance of these drivers varies with the observed latitude and time scale. AMOC, interocean exchanges, and climate changes drive ocean warming at all depths, upper ocean salinification, and freshening in the deep and abyssal ocean in the South Atlantic. Long-term sustained observations are critical to detect and understand these changes and their impacts.

Solar radiation delivers a surplus of heat in the tropics relative to the poles, and the ocean plays a key role in redistributing heat around the Earth to offset this energy imbalance[1–3]. In the ocean, this energy redistribution is largely accomplished through the global overturning circulation, a system of ocean currents that carries seawater with unique thermohaline (temperature-salt) and biogeochemical (e.g., carbon, oxygen, nutrients) signatures within and between ocean basins[4–8]. Along the way, surface, intermediate, deep, and abyssal water masses are created, mixed, blended, and transformed[9–12] following complex and irregular three-dimensional pathways that can vary over seasonal to millennial time-scales[13–23] (Fig. 1; Supplementary Fig. 1 and Supplementary Movie 1).

A distinctive component of the global overturning system is the upper Atlantic Meridional Overturning Circulation (AMOC) cell that transports warm and salty waters from the

[1] Consejo Nacional de Investigaciones Científicas y Técnicas (CONICET), Buenos Aires, Argentina. [2] Departamento de Oceanografía, Servicio de Hidrografía Naval, Buenos Aires, Argentina. [3] CNRS—IRD—CONICET UBA, Instituto Franco-Argentino para el Estudio del Clima y sus Impactos (UMI 3351 IFAECI), Buenos Aires, Argentina. [4] National Oceanic and Atmospheric Administration, Atlantic Oceanographic and Meteorological Laboratory, Miami, FL 33149, USA. [5] Laboratoire de Météorologie Dynamique UMR8539, ENS-PSL/CNRS/Ecole Polytechnique/SU, IPSL Département de Géosciences, Paris, France. [6] Direction Générale de l'Armement, Ingénierie des projets, Paris, France. [7] Scripps Institution of Oceanography, U.C. San Diego, La Jolla, CA, USA. [8] Oceans & Coasts Research Branch, Department of Forestry, Fisheries and the Environment, Cape Town, South Africa. [9] Bayworld Centre for Research and Education, Constantia, Cape Town, South Africa. [10] Oceanography Department, University of Cape Town, Cape Town, South Africa. [11] Oceanographic Institute of the University of São Paulo, São Paulo, Brazil. [12] GEOMAR Helmholtz Centre for Ocean Research Kiel, Kiel, Germany. ✉email: mariapaz.chidichimo@gmail.com

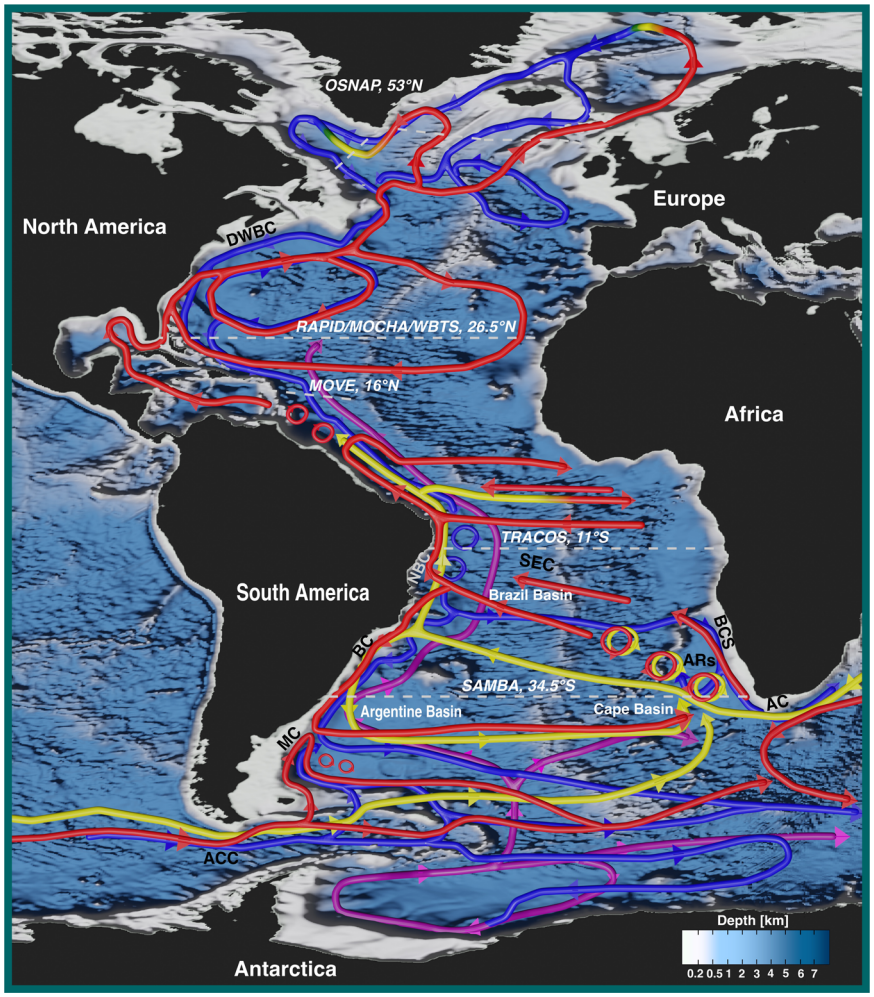

Fig. 1 Idealized schematic of the overturning circulation in the Atlantic Ocean. The schematic represents the pathways of surface (red), intermediate (yellow), deep (blue), and abyssal (purple) waters over the bottom topography (blue shading). Transitions between these colors indicate water mass transformations. Important currents and topographic features mentioned in the text are labeled, and dashed white lines indicate the nominal latitudes of the five Atlantic Meridional Overturning Circulation (AMOC) monitoring arrays (Box 1). AC Agulhas Current, ACC Antarctic Circumpolar Current, ARs Agulhas Rings, BC Brazil Current, BCS Benguela Current System, DWBC Deep Western Boundary Current, MC Malvinas Current, NBC North Brazil Current, SEC South Equatorial Current.

subtropical South Atlantic across the equator towards high latitudes in the North Atlantic where they sink and flow equatorward as cold deep water. Beneath the upper AMOC cell, a weaker abyssal cell exists, that is sourced by the sinking of colder, saline, waters along the ice edge of Antarctica[24] (Fig. 1). Together, these cells carry a maximum of 25% of the net global ocean and atmosphere energy (heat) transport[1,21,25,26]. The upper AMOC cell exerts a tremendous influence on regional weather and global climate both via air-sea exchanges[27–36] and via exchanges with the cryosphere, for instance, through sea-ice melting[37]. AMOC regulates excess anthropogenic heat and carbon storage from the surface into the deep ocean[21,38–40], which modulates the timing and regional impacts of anthropogenic climate change. All greenhouse gas emission scenarios predict that the upper AMOC cell is expected to weaken over the 21st century in response to anthropogenic climate forcing[41], with consequential impacts on heat and carbon uptake and transport, sea level change, the water cycle, changing patterns of atmospheric circulation, extreme events, and marine ecosystems[17,22,42–47]. Extreme freshening in the North Atlantic can trigger a weakening, or a "shutdown" of the upper AMOC cell, which paleoclimatic studies indicate can have vast consequences on the global climate[48–50].

The South Atlantic Ocean plays a unique role in the global overturning circulation because it is the only ocean basin with a net equatorward heat transport[2,7,16,51–57], and it is the basin where the AMOC upper and abyssal cells interact the most (Fig. 1). Furthermore, the South Atlantic acts as the primary conduit for the deeper cold dense water masses formed in the North Atlantic to exit the Atlantic and interact with water masses in other ocean basins[8,10,58–65] (blue pathway in Fig. 1). Interocean exchanges from the Pacific and Indian basins alter the thermohaline and chemical properties of the surface and intermediate water masses (red and yellow pathways, respectively, in Fig. 1) as they are formed, transformed, and transported through the South Atlantic on their way to the North Atlantic[65,66]. Cold and fresh water masses from the Pacific Ocean flow through Drake Passage[6,58,65,67] and largely traverse eastward to meet the warm and salty water masses from the Indian Ocean flowing through the gap between South Africa and the Antarctic continent (Fig. 1). These flows primarily enter the South Atlantic through the Cape Basin region via mesoscale eddies referred to as Agulhas Rings and the Benguela Current System (BCS)[59,63,68,69] to feed into the upper limb of the AMOC[59,60,65–67,70,71]. Interocean exchanges induce two regions of high mesoscale variability in the South

Box 1 | Observing the overturning circulation in the South Atlantic

The strength of the upper AMOC cell is traditionally denoted as the maximum northward volume transport across a particular latitude[96,247] and is measured in Sverdrups (hereafter Sv; 1 Sv equals 10^6 m^3 s^{-1}). More specifically, AMOC volume transport is calculated as the double integral of the meridional (north-south) component of velocity between the western and eastern boundaries of the basin, and from the sea surface down to the depth where the zonally and vertically integrated flow in the upper AMOC cell changes from northward to southward (nominally around a depth of 1000 m or pressure of 1000 dbar)[15,16,97,98,100,164–166,233,247]. Direct velocity measurements at all required space and time-scales are infeasible, so the overturning volume transport is computed as a sum of Ekman (wind-driven), baroclinic (buoyancy-difference driven), and barotropic (pressure-difference driven) components. The Ekman component can be estimated from global wind datasets. The baroclinic component is derived from trans-basin ocean density or dynamic height profile data. The barotropic component is estimated using a combination of one or more techniques: making the assumption of net-zero volume (mass) transport, prescribing Bering Strait transport, or using bottom pressure differences or a reference velocity[15,16,97,98,100,164–166,233,247].

Combining flow estimates with property observations allows for the estimation of the property transports. Early estimates of volume, heat (measured in Petawatts or PW), and freshwater (measured in Sv) transports in the South Atlantic were obtained from high horizontal resolution (10–50 km) shipboard measurements made along snapshot trans-basin transects. Expendable bathythermograph (XBT) transects, which measure temperature in the upper ~850 m, have been repeated quarterly since the 2000s. Combined with historical hydrographic observations, XBT transects are used to examine the seasonal-to-interannual variability of volume and heat transports[16,53,233,248]. A few repeated full-depth conductivity-temperature-depth (CTD) transects have provided estimates of volume, heat, and freshwater transports that can be compared over the decades[56,166,167] and combined with inverse models to produce globally-balanced mean transport estimates[61,184,249,250]. Ship-based transport estimates are considered "instantaneous snapshots", but in reality, each trans-basin section can take weeks to months to complete.

More recently, daily estimates of the volume transport by the overturning circulation[15,97,98,100], their heat transport[55], and associated boundary current transports[85,113,122,177,251] have been obtained from moored arrays. These arrays have the benefit of resolving high-frequency variations, and in some cases, the full-depth structure of the water column but have the disadvantage of limited geographic availability (i.e., most moorings are concentrated near the coasts and at select latitudes). These moorings include pressure-recording inverted echo sounders (PIES), which observe most of the water column acoustically, tall moorings which directly sample temperature, salinity, and/or velocity at discrete depths from near the ocean surface to the seafloor, acoustic Doppler current profiler (ADCP) moorings which directly measure velocity profiles over a limited depth range or bottom pressure gauges. Most moorings are used to estimate baroclinic or barotropic transports, and moorings with current meters or ADCPs can reference those transports or estimate boundary current contributions. During the past decade, moored arrays that have been maintained at both boundaries at 11°S[122,123,178] and at 34.5°S[84,85,101,113,177,251] have evolved into the trans-basin TRopical Atlantic Circulation and Overturning at 11°S (TRACOS) array and the SAMoc Basin-wide Array (SAMBA), respectively[15,97,98,100,101].

Multi-decade time series of AMOC volume and heat transports have been derived at various latitudes in the South Atlantic using satellite altimetry measurements combined with in situ data from Argo profiling floats, XBTs, and/or CTDs[57,164,165,239]. A sea surface temperature-based AMOC proxy was also developed[252], which allows for analysis of monthly AMOC variability from the early 1870s to the present at multiple latitudes in the South Atlantic, providing an observation-based glimpse of long-term AMOC variations. Proxy and partial-basin estimates are not as accurate as full-depth continuous trans-basin measurements, but they are cost-effective and allow us to study AMOC at a wide range of time and space scales.

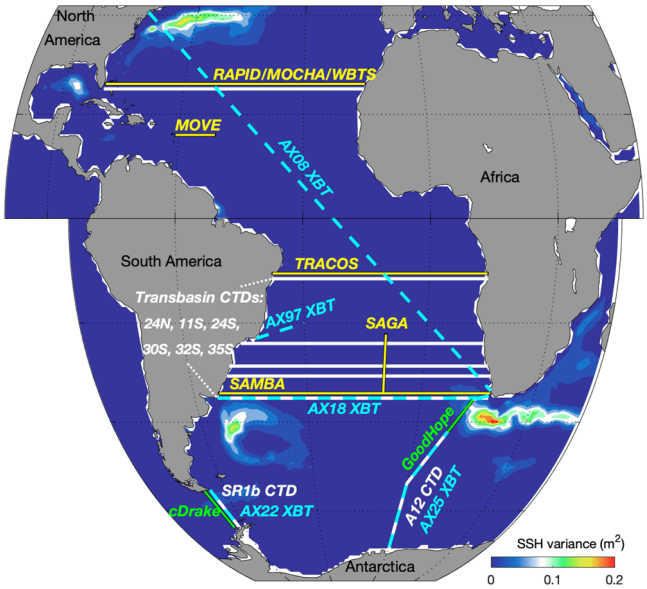

Schematic of the SAMOC observing system, including linkages to the AMOC-related observing systems with other ocean basins via interocean exchanges.

Moored transport arrays in the tropical and subtropical Atlantic are identified as yellow solid lines (SAMBA, TRACOS, SAGA, MOVE, and RAPID/MOCHA/WBTS). Past AMOC-related arrays in Drake Passage (cDrake) and south of South Africa (GoodHope) are identified as green solid lines. Repeat XBT transects are indicated by dashed light blue lines (AX08, AX18, AX22, AX25, AX97), and repeated CTD lines are indicated by white solid lines (24°N, 11°S, 24°S, 30°S, 32°S, 34.5°S, SR1b, A12). Color shading indicates elevated regions of sea surface height (SSH) variance in units of m^2 (i.e., regions with strong eddies and high mesoscale variability).

Box 2 | Observing South Atlantic interocean exchanges from the Pacific and Indian basins

Drake Passage has been uniquely well-sampled in the Southern Ocean and has been the focus of a number of field campaigns beginning with the International Southern Ocean Studies (ISOS) program[253]. The cDrake study of Antarctic Circumpolar Current (ACC) transport and dynamics deployed 41 bottom-moored current and pressure-recording inverted echo sounders (CPIES) for a period of 4 years (2007–2011)[206] (Box 1). The cDrake array comprised a transport line spanning the full passage and a local dynamics array situated in the northern passage eddy kinetic energy maximum. Sustained observations in Drake Passage include a long-term (20+ years) time series of upper ocean temperature, salinity, and current observations, as well as concurrent shipboard meteorological and CO_2 sampling, from the year-round transits of the U.S. Antarctic Program supply vessel, *ARSV Laurence M. Gould*[254]. This ship crosses Drake Passage on a spatially near-repeated transect on average 20 times a year and provides a unique data set of underway continuous SADCP, meteorological, and carbon measurements, and ~6 transects per year, including discrete XBT profiles at relatively high temporal and spatial resolution (designated AX22 in Box 1). The WOCE and GO-SHIP repeat-hydrography line SR1b has been occupied almost annually since 1993–1994, providing one of the longest Southern Ocean time series of full-depth measurements of temperature and salinity, enabling investigation of interannual to decadal changes in water masses of both the upper and lower cells of the overturning circulation[189].

There have been several experiments and programs to measure contributions to Indo-Atlantic interocean exchange from the Agulhas Leakage and its variability, although sustained and comprehensive observing programs have proven difficult. These include the GoodHope program[230,255,256], repeated GO-SHIP survey line A12, the high-resolution AX25 XBT transect, mooring arrays in the Atlantic Ocean, including SAMBA[16,62,84,85,99,100] (Box 1), and the earlier Agulhas South Atlantic Thermohaline Transport Experiment (ASTTEX)[257] and BEnguela Source and Transport (BEST)[258,259] arrays, as well as mooring arrays in the Agulhas Current that include the Agulhas Current Time-series (ACT) and Agulhas System Climate Array (ASCA) programs[260–262].

Atlantic, the Confluence of the Brazil Current (BC) and Malvinas Current (MC) on the western boundary and the Agulhas Leakage on the eastern boundary (areas with elevated sea surface height variance in Box 1). These regions of high mesoscale activity and air-sea interactions contribute to the formation of new water masses[9–11,65]. At the deepest layers (purple pathway in Fig. 1), newly formed abyssal waters of Antarctic origin flow northward into the Argentine and the Brazil Basins[72–76], cross the equator, and ultimately mix with other deep and abyssal waters.

While many of the constituent flows of AMOC are meridional (north-south) in orientation, zonally oriented (east-west) flows can play an important role in linking different AMOC pathways. This is particularly apparent in the South Atlantic, where the lower limb of the upper AMOC cell, marked by North Atlantic Deep Water (NADW) carried southward by the Deep Western Boundary Current (DWBC), splits around 20°S and loses a small portion of its flow eastward across the basin toward the African coast[12,64,77,78] (blue pathway in Fig. 1), although it remains in question whether this eastward NADW flow continues into the Cape Basin or recirculates around the Angola Basin[79]. The upper limb of the AMOC transports surface and intermediate water masses northwestward across the basin via Agulhas Rings and through the BCS and South Equatorial Current (SEC)[10,62,80–85] (red and yellow pathways, respectively, in Fig. 1).

Deep water formation associated with the AMOC at high latitudes in the North Atlantic has been linked to changes in local stratification and in the thermohaline properties of the upper limb of the AMOC in the South Atlantic[10,16,65]. Theory and models have suggested the direction of the meridional freshwater transport by the upper AMOC cell at the southernmost border of the South Atlantic (i.e., 34.5°S) is a control parameter on the mono- or bi-stability of AMOC[86–91]. In a monostable system, AMOC imports freshwater into the South Atlantic. In a bistable system, where AMOC exports freshwater poleward out of the South Atlantic, it is possible to abruptly switch from an "AMOC on" to "AMOC off" state causing abrupt regime shifts in the water cycle and regional weather patterns leading to planetary climate impacts[47].

Over the past two decades, the international scientific community has made numerous advances in the study of the AMOC due to the growth of long-term observing programs at various latitudes in the Atlantic basin[15,16,19,92–98]. These observational programs combined with models have revolutionized our understanding of the mean structure and pathways of the AMOC, its variability on time-scales ranging from days to decades, and its drivers. While the development of a comprehensive AMOC observing system in the South Atlantic has lagged behind the North Atlantic, there is now a concerted international effort focused on studying the role of the South Atlantic dynamics in driving AMOC changes and regional climate variability. This international South Atlantic Meridional Overturning Circulation (SAMOC) initiative began in 2007[10,99–101]. The SAMOC observing system consists primarily of purposely designed trans-basin and boundary current mooring arrays and synoptic ship-based hydrographic observations in the South Atlantic and in the regions of interocean exchanges (Box 1; Box 2). SAMOC also leverages global satellites, Argo profiling floats, and surface drifting buoys, which provide key observations that are useful for overturning studies. The goal of the SAMOC initiative is to monitor climatically relevant oceanic fluxes of mass, heat, and freshwater, and provide observations critical to validate and improve numerical models and climate predictions[102–104].

Several recent review articles have summarized what we have learned from AMOC observing systems, but they primarily focused on the North Atlantic[19,95,96]. The only review article focused solely on the South Atlantic circulation precedes major findings from the SAMOC initiative[10]. The present review will highlight recent advances revealed by the SAMOC observing system along with newly developed observational analysis techniques. The review will serve to demonstrate the critical role of long-term sustained observations for detecting and understanding circulation variability in this region across a multitude of time-scales, and our present ability to model some of the changes. Specifically, we will focus on the insights gained into changes in circulation, water masses, transports, boundary currents, and eddy-rich interocean exchanges. These changes must be monitored and studied to continue to assess and understand their known (and still unknown) impacts on climate phenomena such as precipitation patterns and extreme events (e.g., marine heat waves, hurricanes), sea level rise, and temperature and salinity trends. Finally, we present a summary and our perspective on the remaining key outstanding research questions and identify observational gaps that challenge our current ability to answer these questions.

Recent progress in understanding South Atlantic water masses formation, transformation, and pathways

Properties of South Atlantic water masses have been studied since the earliest oceanographic surveys, conducted by Germany[51,105,106], and have been actively coordinated internationally since the late 1950s[107–109]. Since then, the World Ocean Circulation Experiment (WOCE) in the 1990s, the Climate

and Ocean—Variability, Predictability and Change (CLIVAR) project in the 2000s, and more recently, the Global Ocean Ship-based Hydrographic Investigations Program (GO-SHIP) have continued with full-depth sampling and establishing best practices for repeated decadal hydrographic transects[110] (Box 1). With the expansion of the international Argo program in the 2000s[111,112], as well as research cruises in support of the SAMOC initiative (Box 1), hydrographic observations in the region have increased dramatically in the last 20 years[12,56,85,113–115]. As of March 2022, there were over 540 active Argo floats (including ~210 biogeochemical Argo floats and a dozen deep Argo floats) collecting water property profiles (mostly in the upper 2000 m) in the South Atlantic sector between the equator and 60°S. Beyond estimating AMOC transports (Box 1), these observations have been key in assessing the distributions, properties, and large-to-mesoscale (1000 to 50 km) ocean dynamics in the basin. Moreover, by acquiring repeated hydrographic data that spans multiple decades, it is possible to assess how these waters are affected by climate change.

A simple picture of AMOC water mass pathways in the South Atlantic involves alternating northward and southward flows along surface/intermediate, deep, and abyssal layers which compensate one another, such that the total flow across any full-depth, trans-basin line approximately balances at long timescales. These flows either move in the same density layers (adiabatic) or they eventually cross them (diabatic). Other ocean circulation systems can impact, and can be impacted by, the overturning circulation, such as the South Atlantic subtropical gyre[32,116] and the subtropical cells[115]. Due to diverse air-sea interaction processes, the upper layer is composed of water masses originating at the surface from the tropics (Surface Water), subtropics (Central Water), and the circumpolar (Antarctic Intermediate Water, AAIW) regions. These waters can be formed locally and can be influenced by waters from the Pacific, Indian, and Southern Ocean, and their complex distributions and pathways are regulated by the overturning circulation (Fig. 1). This constitutes the time-mean background, with which the upper limb of the upper AMOC cell interacts as it makes its way to the North Atlantic Ocean. The lower limb of the upper AMOC cell involves the export of NADW to the Southern Ocean where it joins the Antarctic Circumpolar Current (ACC). NADW export is compensated by a northward flow of surface, central, and intermediate waters through the upper layers in the South Atlantic and across the equator, and by the northward flow of Antarctic Bottom Water (AABW) carried by the abyssal cell[58,69,74,76,114,117–119]. Heat and freshwater transported by these interocean exchanges substantially impact the Atlantic Ocean as a whole[58,65,66,69,120].

How AMOC water mass pathways in the South and North Atlantic Ocean are linked, and in particular how water masses cross the equator, is also a topic of considerable interest. For deep water masses, the main route from the North Atlantic to the South Atlantic is thought to be via the DWBC with some zonal detours within the deep equatorial current system[67,121] (Fig. 1). For warm surface and intermediate waters flowing northward from the South to the North Atlantic, the dominant pathway along the western boundary via the North Brazil Under Current (NBUC) and North Brazil Current (NBC) system is often referred to as the "direct" pathway[122–125]. The "direct" pathway reaches the Caribbean Sea via the NBC retroflection region, where NBC rings are spun off (Fig. 1). The "indirect" interior pathway consists of the complex zonal equatorial current system, fed in part by the NBC retroflection, and interior northward transport in the subtropical cells in the tropical Atlantic which also plays an important role in the AMOC[115] (Fig. 1).

The connection to the neighboring ocean basins adds complexity to the South Atlantic's water mass configuration. In the subtropical South Atlantic, between 35°S and 11°S, recent hydrographic surveys have provided more detailed descriptions and sources of the water masses[12,56,74,84,85,114,126] (Fig. 2c; Table 1). South Atlantic Central Waters (SACW) are produced locally as they originate from the subduction of subtropical Mode Waters in hotspots of air-sea interaction and eddy activity in the southwestern Atlantic at the Brazil-Malvinas Confluence (BMC) and the southeastern Atlantic[127,128] (Box 1). These two regional hotspots also encompass pathways whereby relatively fresh and highly oxygenated intermediate waters enter the South Atlantic. In the BMC, a regional variety of Subantarctic Mode Water is subsequently transformed into a fresh Atlantic variety of AAIW[129–131], and a saltier AAIW variety that has Indian origin enters the South Atlantic through the Agulhas Leakage and BCS[56,68,80,131,132] (Fig. 2a–c).

Between ~1100 and 1600 dbar (~1100–1600 m depth), an oxygen minimum layer of Upper Circumpolar Deep Water (UCDW; Fig. 2c) originating from Drake Passage flows equatorward in the Cape Basin and southward in the Argentine Basin[56], while the trans-basin zonally-integrated UCDW transport is southward at 34.5°S. At greater depths, two different veins of NADW flow southward. Near the western boundary, NADW has more pristine properties (saltier and warmer) due to a more direct pathway from its North Atlantic source region, than the vein hugging the African continental slope (fresher and colder), which has followed a more complex and longer route connected through an interior pathway[64,67,77,78,85,117].

Lower Circumpolar Deep Water (LCDW) and Weddell Sea AABW both flow northward along the western side of the Brazil Basin. However, the northward spreading of LCDW and AABW is blocked on the eastern side of the Mid-Atlantic Ridge by the Walvis Ridge, and only older varieties of abyssal waters are found with no clear interior pathway[7,56,60,80,114,129] (Figs. 1, 2). Abyssal water masses are mixed on their way to the north and become harder to track and distinguish from other water masses near the tropical region. Although there are some inter-study differences as to which isopycnal marks the boundary between NADW, LCDW, and AABW[12,56,133], waters with neutral densities larger than 28.15 kg m^{-3} are classified as AABW, with younger waters in the western portion of the basin and older waters in the eastern portion (Table 1).

Warming and salinity changes detected from the surface to the abyssal ocean

Recent observational and modeling studies suggest that a reduction in the strength of the AMOC could lead to an additional warming of South Atlantic sea surface temperatures relative to cooling of North Atlantic sea surface temperatures[35,134,135] and a weakened salinity divergence between the South and North Atlantic, resulting in a net salt gain in the South Atlantic[136].

Tracking water mass characteristics and their changes over space and time can help to determine water mass pathways and understand their origins and impacts. As an example, a 21st-century climate projection predicts increased Agulhas leakage in response to the poleward shift of the Southern Hemisphere westerlies, which will cause an increased transport of warm and salty water from the Indian into the South Atlantic Ocean[81]. An upper ocean warming and salinification trend have been traced by observations through the South Atlantic[137] (Fig. 3a, c) up to the western boundary at 11°S[122] from the early 2000s to the early 2010s, apparently consistent with the above-mentioned scenario. Adding more nuance, a more recent modeling study[65] showed

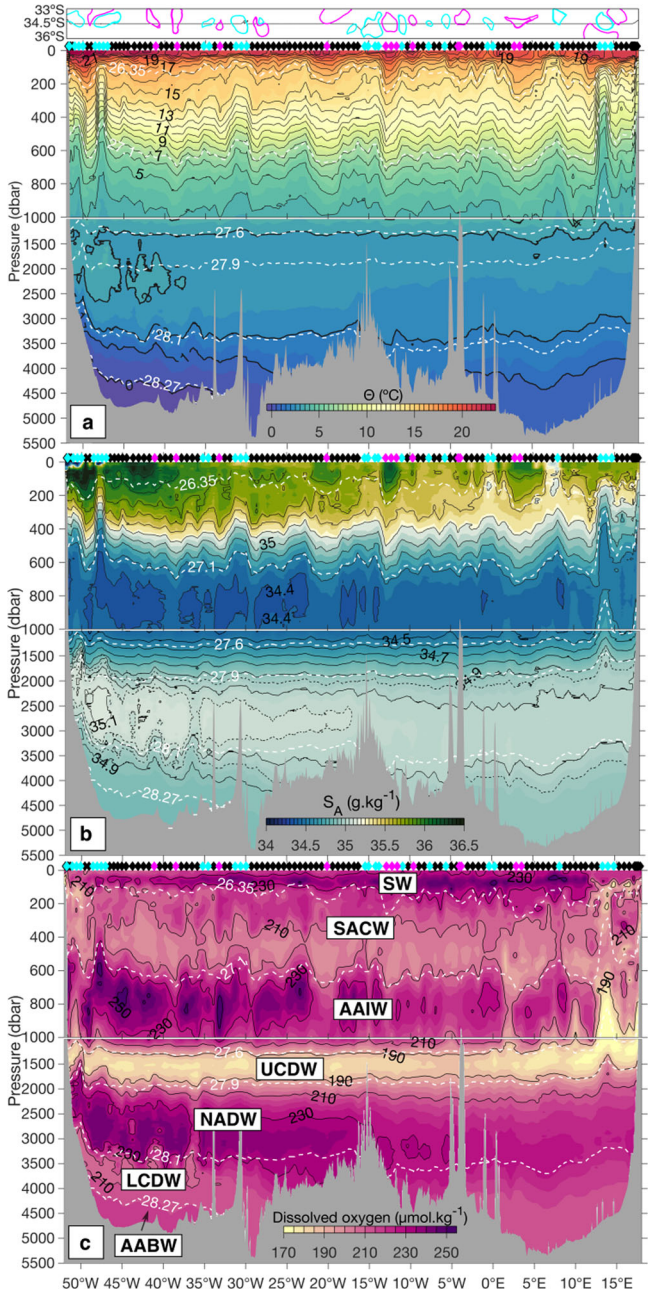

Fig. 2 Water properties observed in the subtropical South Atlantic. **a** Conservative temperature (Θ, °C), **b** Absolute salinity (S_A, g kg^{-1}), and **c** Dissolved oxygen (O_2, µmol kg^{-1}) along the SAMBA section at 34.5°S in January 2017[56]. The neutral density layers (γ^n, kg m^{-3}) bounding each water mass are shown in white dotted curves in all panels. A map showing the location of anticyclonic and cyclonic eddies crossed during the cruise in magenta and cyan, respectively, is shown on top of panel **a**. The diamonds indicate the location of the 128 CTD profiles, colored in black, magenta and cyan depending if they were occupied outside, or within an anticyclonic or a cyclonic eddy, respectively. The upper 1000 dbar are vertically stretched. SW Surface Water, SACW South Atlantic Central Water, AAIW Antarctic Intermediate Water, UCDW Upper Circumpolar Deep Water, NADW North Atlantic Deep Water, LCDW Lower Circumpolar Deep Water, AABW Antarctic Bottom Water.

that the combined effect of a weakening fresh South Pacific inflow and increasing salty Indian inflow on the northward AMOC transport in the NBUC region might be driving the observed salinification from 2000–2009 (Fig. 3c).

Table 1 Defining features of water masses in the subtropical South Atlantic.

Water mass	γ^n [kg m^{-3}]	Θ [°C]	S_A [g kg^{-1}]	O_2 [µmol kg^{1}]
SW	<26.35	17.85	35.74	228
SACW	26.35–27.10	11.63	35.22	211
AAIW	27.10–27.60	4.34	34.48	216
UCDW	27.60–27.90	2.88	34.76	185
NADW	27.90–28.10	2.47	35.02	223
LCDW	28.10–28.27	1.07	34.92	216
AABW	>28.27	−0.07	34.85	215

Neutral density ranges (γ^n), conservative temperature (Θ), absolute salinity (S_A), and dissolved oxygen concentration (O_2) per water mass across 34.5°S in the Atlantic[56].
SW Surface Water, *SACW* South Atlantic Central Water, *AAIW* Antarctic Intermediate Water, *UCDW* Upper Circumpolar Deep Water, *NADW* North Atlantic Deep Water, *LCDW* Lower Circumpolar Deep Water, *AABW* Antarctic Bottom Water.

Near the surface, the observed ocean warming associated with ongoing planetary warming is fairly ubiquitous in the South Atlantic from 1980 to 2020[138] (Fig. 3a), with maximum warming, on the order of 1.2 °C decade^{-1} in the upper 700 dbar (~700 m depth) (Fig. 3a), found along the BC and in the BMC region[138–140]. Upper ocean salinity has also increased from the 1950s to the 2000s (Fig. 3c), with large increases in high salinity regions such as in the sea surface salinity maximum found between 0° and 30°S[141–143] and in the BC and BMC region where an increase on the order of 0.15 psu decade^{-1} (comparable to 0.15 g kg^{-1} decade^{-1}) in the upper 700 m is observed (Fig. 3c).

The thermocline waters most affected by long-term warming signals are the mode and intermediate waters since they are formed at the surface in both the subpolar and subtropical regions and then penetrate the South Atlantic subtropical gyre at depth[144–147]. A recent study found that about 1.5×10^{22} J of heat was converging in the South Atlantic in the $\sigma_\theta = 26.0–27.0$ kg m^{-3} potential density layer (roughly between 200 and 700 m depth) from 2006 to 2015[148] (Fig. 3a). Despite its small area, upper ocean warming in the South Atlantic accounts for roughly 10% of global upper ocean warming. Some of this excess heat has been taken up by subtropical Atlantic mode waters since nearly 1980, which then ventilate the main thermocline and transport heat away from the surface[128,138,148,149]. South Atlantic AAIW properties also show significant warming, and their salinity seems to be decreasing over the past few decades[148,150] (Fig. 3b, d), due to competing influences from increased Agulhas Leakage and declining South Pacific inflow (salinification) vs. the intensification of the hydrological cycle (freshening) (Fig. 3d). In the mid-depth layer between AAIW and NADW, warming on the order of 0.044 °C decade^{-1} and freshening on the order of 0.006 g kg^{-1} decade^{-1} has been observed from 2006 to 2015[151] (Fig. 3b, d). Although temperature and salinity changes in the ocean interior can be due to isopycnal heave (i.e., vertical movement of density layers), this was not the case for this mid-depth layer. Rather, changes were attributed to anomalous southward advection by the AMOC[151].

Decadal and longer time-scale temperature and salinity trends associated with deep (2000–4000 m) and abyssal (4000–6000 m) water masses are relatively small and can be obscured by sub-decadal time-scale variability[38,152–156]. However, in these deep and abyssal layers, noticeable warming and freshening trends are emerging in the South Atlantic that is either expression of decadal and multi-decadal variability or of anthropogenic climate change[12,73,157–160]. More studies are needed to determine whether these trends, should they persist, are due to changes in the properties of NADW and AABW, or their relative abundance and their vertical distributions[158,161]. The observed AABW warming is strongest in the Southwest Atlantic where the younger variety

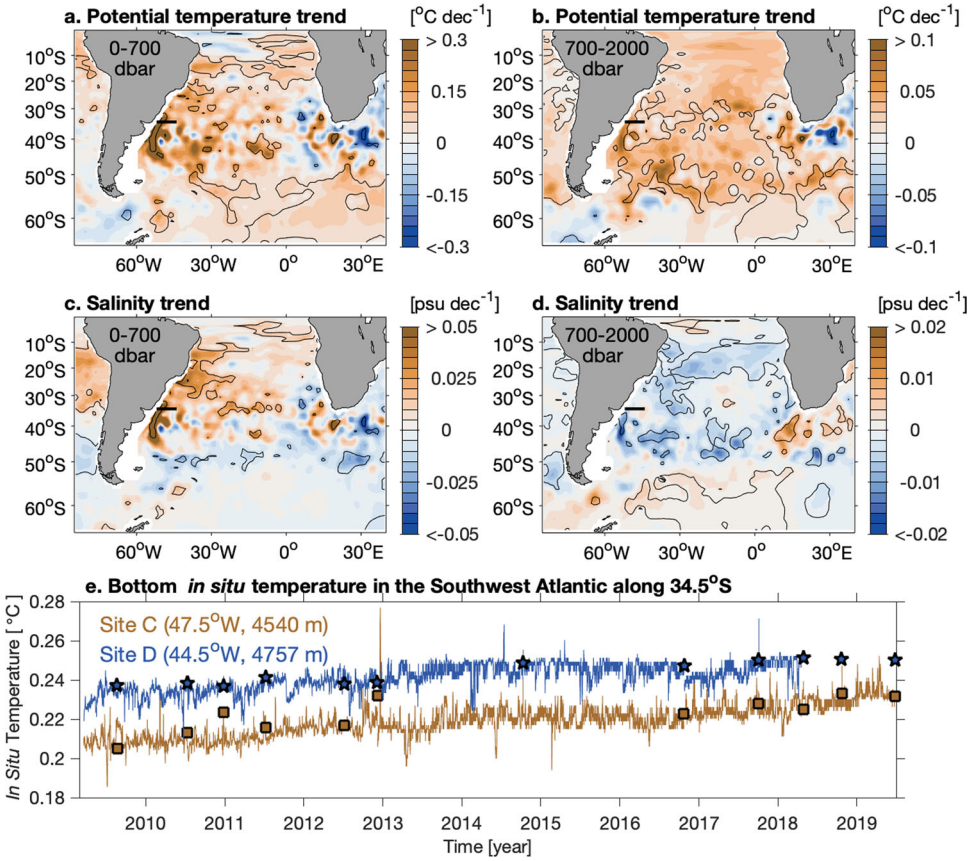

Fig. 3 Temperature and salinity trends in the South Atlantic. a, **b** Trends of temperature averaged over the top 700 dbar and between 700 and 2000 dbar. **c**, **d** Trends of salinity averaged over the top 700 dbar and between 700 and 2000 dbar. The decadal linear trends in (**a**–**d**) are computed from annual Argo climatology[246] for the years 2004–2018. Black contour lines indicate trends that are significant at the 90% confidence level. The black horizontal line indicates the position of the western SAMBA moorings at 34.5°S. **e** In situ hourly bottom temperature data from western SAMBA moorings[75] at 47.5°W (Site C; brown curve) and 44.5°W (Site D; blue curve) from March 2009 to June 2019. Squares and stars are corresponding hydrographic measurements during research cruises used to calibrate the mooring data at 47.5°W and 44.5°W, respectively.

of AABW has to cross through the Vema Channel near 31°S, 39°W. Steady and significant AABW warming has been observed from moored observations and hydrographic data in the Vema Channel of about 0.02 °C decade^{-1} since the 1980s, which has accelerated to approximately 0.026 °C decade^{-1} since 2005[76,162]. Abyssal warming of 0.02 ± 0.01 °C decade^{-1} was also observed over the period 2009–2019 from continuous hourly measurements from two moored instruments located near the 4500 m and 4800 m isobaths in the northwestern Argentine Basin along the SAMBA line at 34.5°S[75] (Fig. 3e). Closer to the tropics, abyssal warming on the order of 0.02 to 0.03 °C decade^{-1} was observed in the Brazil Basin between 0°–30°S, 40°W–10°W from recent deep Argo data (2019–2020) and hydrographic data spanning multiple decades[163], and in the western tropical Atlantic from multi-decadal repeat hydrographic cruises[12].

Quantifying energetic South Atlantic meridional volume, heat, and freshwater transports

As described in Box 1, estimates of AMOC and associated meridional heat transport (MHT), and/or freshwater transport from the surface to the seafloor across the South Atlantic have been derived from repeated CTD sections, XBT transects, inverse models, blended in situ and satellite data, and moorings at multiple latitudes in the South Atlantic from 35 to 11°S with different record lengths, time and space scales, and accuracies. Key recent findings are synthesized and described below (Table 2, Fig. 4).

Time-mean estimates of the upper AMOC cell and full-depth MHT at various latitudes determined from trans-basin shipboard data and also a ~30-year (1993-present) blended product of in situ and satellite observations (Table 2) exhibit a wide range of northward volume transport values ranging from 11.7 to 28.0 Sv[126,164] with MHT ranging from 0.27 to 0.92 PW[56,164] and large standard deviations ranging from 1.4 to 4.6 Sv and from 0.10 to 0.22 PW, respectively[56,164]. Concurrent AMOC estimates at multiple latitudes reveal that both the variability of AMOC and MHT decrease northward from 34.5 to 20°S[19,57,164,165] (Fig. 4d, e).

Using data from the TRACOS mooring array at 11°S in the tropical Atlantic, the seasonal and shorter time-scale variability of the upper AMOC cell was investigated over the period 2013–2018[98] (Table 2; Fig. 4a). A pronounced annual (seasonal) cycle has been observed at 11°S with an amplitude of 8 Sv attributed to the variability of both the upper ocean geostrophic and Ekman transport. Based on Argo data and repeated shipboard velocity measurements combined with satellite winds, the time-mean upper AMOC flow at 11°S was estimated as 16.4 Sv[115].

In the subtropical South Atlantic, the first estimates of the daily upper cell AMOC transport were obtained using measurements from a pair of PIES moorings near the 1300 m isobath on either flank of the South Atlantic at 34.5°S deployed as part of the pilot configuration of SAMBA[15,100]. These analyses have demonstrated that the AMOC is highly variable at time-scales ranging from a few days to a year. Using nine of the SAMBA PIES moorings that

Table 2 Estimates of AMOC and MHT (temporal mean ± standard deviation) at different latitudes in the South Atlantic in the published literature from 2011 to the present.

Sources	Latitude	AMOC [Sv]	MHT [PW]	$r_{(AMOC, MHT)}$	Data	Time	Resolution, filter
Bryden et al.[166]	24°S	16.5	0.40	N/A	GO-SHIP section	02/1983–03/1983	Snapshot
	24°S	21.5	0.70	N/A		03/2009–04/2009	Snapshot
Dong et al.[234]	34°S	17.9 ± 2.2	0.55 ± 0.14	0.76	XBT; WOA	2002–2008	Quarterly transects
Garzoli et al.[16]	35°S	18.1 ± 2.3	0.54 ± 0.14	0.73	XBT; WOA	2002–2011	Quarterly transects
Dong et al.[165]	20°S	17.2 ± 1.7	0.71	N/A	XBT—altimetry	1993–2006	Monthly data
	25°S	18.2 ± 1.8	0.68	N/A			
	30°S	20.6 ± 2.2	0.67	N/A			
	34.5°S	19.5 ± 3.5	0.67	N/A			
Majumder et al.[164]	20°S	17.1 ± 2.5	0.53 ± 0.16	N/A	Argo—altimetry	2000–2014	Monthly data
	25°S	28.0 ± 2.8	0.92 ± 0.15	N/A			
	30°S	23.4 ± 4.6	0.76 ± 0.22	N/A			
	35°S	20.7 ± 4.2	0.66 ± 0.21	N/A			
Meinen et al.[100]	34.5°S	21.3 ± 8.7	N/A	N/A	PIES; Model (time-mean)	03/2009–12/2010	Daily data; 72 h low-pass filtered
Meinen et al.[15]	34.5°S	14.7 ± 8.3	N/A	N/A	PIES; Model (time-mean)	03/2009–04/2017	Daily data; 72 h low-pass filtered
Hernández-Guerra et al.[126]	30°S	12.1 − 14.7	N/A	N/A	GO-SHIP sections	11/2003	Snapshot
	30°S	11.7 − 17.7	N/A	N/A		09/2011	Snapshot
Kersalé et al.[97]	34.5°S	17.3 ± 15.5	N/A	0.96	PIES; Model (time-mean)	09/2013–07/2017	Daily data; 72 h low-pass filtered
Kersalé et al.[55]	34.5°S	N/A	0.5 ± 0.8	0.96	PIES + in situ + altimetry; Model (time-mean)	09/2013–07/2017	Daily data; 72 h low-pass filtered
Manta et al.[56]	34.5°S	15.64 ± 1.39	0.27 ± 0.10	N/A	GO-SHIP section	01/2017	Snapshot
Dong et al.[57]	20°S	16.6 ± 2.1	0.62 ± 0.16	0.90	in situ + altimetry	1993–2020	Monthly data
	25°S	19.0 ± 2.2	0.66 ± 0.16	0.97			
	30°S	18.9 ± 2.0	0.62 ± 0.15	0.90			
	34.5°S	18.3 ± 3.5	0.57 ± 0.21	0.93			
Herrford et al.[98] (time series) with time-mean from Tuchen et al.[115]	11°S	16.4 ± 6.4	N/A	N/A	BPR + satellite (SLA, winds); Argo + satellite winds (time-mean)	07/2013–02/2018	5-days resolution

The reference citation, data, and time period used are also indicated (month information is given if the record does not span a full year). Positive transport values indicate northward transport. The correlation ($r_{AMOC,MHT}$) values between AMOC and MHT time series are included when available.
AMOC Atlantic Meridional Overturning Circulation, *MHT* Meridional Heat Transport, *SLA* Sea Level Anomaly, *BPR* Bottom Pressure Recorder, *WOA* World Ocean Atlas.

had continuous daily observations from September 2013 to July 2017, a more recent study resolved the daily AMOC transports from the surface down to ~4700 dbar (~4700 m)[97], and also found a highly variable upper AMOC cell (black solid curve in Fig. 4b). This improved and updated AMOC estimate allows for better accuracy of the volume transport estimates as well as the ability to attribute the sources of the signals. A key new result from this study was the estimation of the daily time-varying strength of the abyssal cell (defined as the maximum southward flow between 3000 dbar and the seafloor beneath the upper AMOC cell; black dashed curve in Fig. 4b); previously, this cell has only been determined from once-a-decade snapshot estimates from basin-wide sections[126,166–168] or combinations of hydrographic sections with inverse models[61,169]. The flows in the upper and abyssal cells vary independently, and the upper cell circulation (time-mean of 17.3 Sv northward transport, standard deviation of 15.5 Sv) is more energetic than the abyssal-cell circulation (time-mean of −7.8 Sv southward transport, standard deviation of 6.2 Sv) at all time-scales resolved over this 4-year observational period[97] (Table 2; Fig. 4b). Of interest, historical observations yielded ~7 Sv of northward-flowing AABW[170] (~4 Sv through the Vema Channel[171] and ~3 Sv through the Hunter Channel[172]), which matches remarkably well with the independent SAMBA estimate of −7.8 ± 2.7 Sv (time-mean ± bias error) for the southward upper limb of the abyssal cell[97], assuming that this flow is compensated by the AABW in the lower limb of the abyssal flow. In addition, the amplitude of the upper AMOC seasonal cycle was 7 Sv using nine moorings[97], compared to an amplitude of only 4 Sv when using two moorings[15]. SAMBA has continued to expand over time and now has on the order of twenty moorings[97], but an AMOC estimate has yet to be generated using more than nine mooring sites.

Measurements from SAMBA have revealed that the variations in the upper AMOC cell at 34.5°S are somewhat more complex than what has previously been observed in the subtropical North Atlantic on intraseasonal, seasonal, and interannual time-scales[13,18,19,92–94,153,173–175]. This is because density and pressure variations on both sides of the Atlantic at 34.5°S are important to the AMOC variations at all time-scales, from daily to interannual, based on the observations collected to date. Furthermore, at 34.5°S it is critical to independently observe the Ekman, baroclinic, and barotropic components of the AMOC volume and heat transports, as all contribute roughly equally to the semi-annual AMOC cycle, and both the baroclinic and barotropic components can dominate interannual variations in different years[15,55,97]. In contrast to the importance of both the Ekman and geostrophic contributions at both boundaries to the AMOC at 34.5°S, at 11°S the annual (seasonal) AMOC variations are primarily forced by geostrophic variations with the largest seasonal pressure variability on the eastern boundary, and secondarily by winds[98]. Despite some dynamical differences at 11°S and 34.5°S, the amplitude of the seasonal cycles observed by the

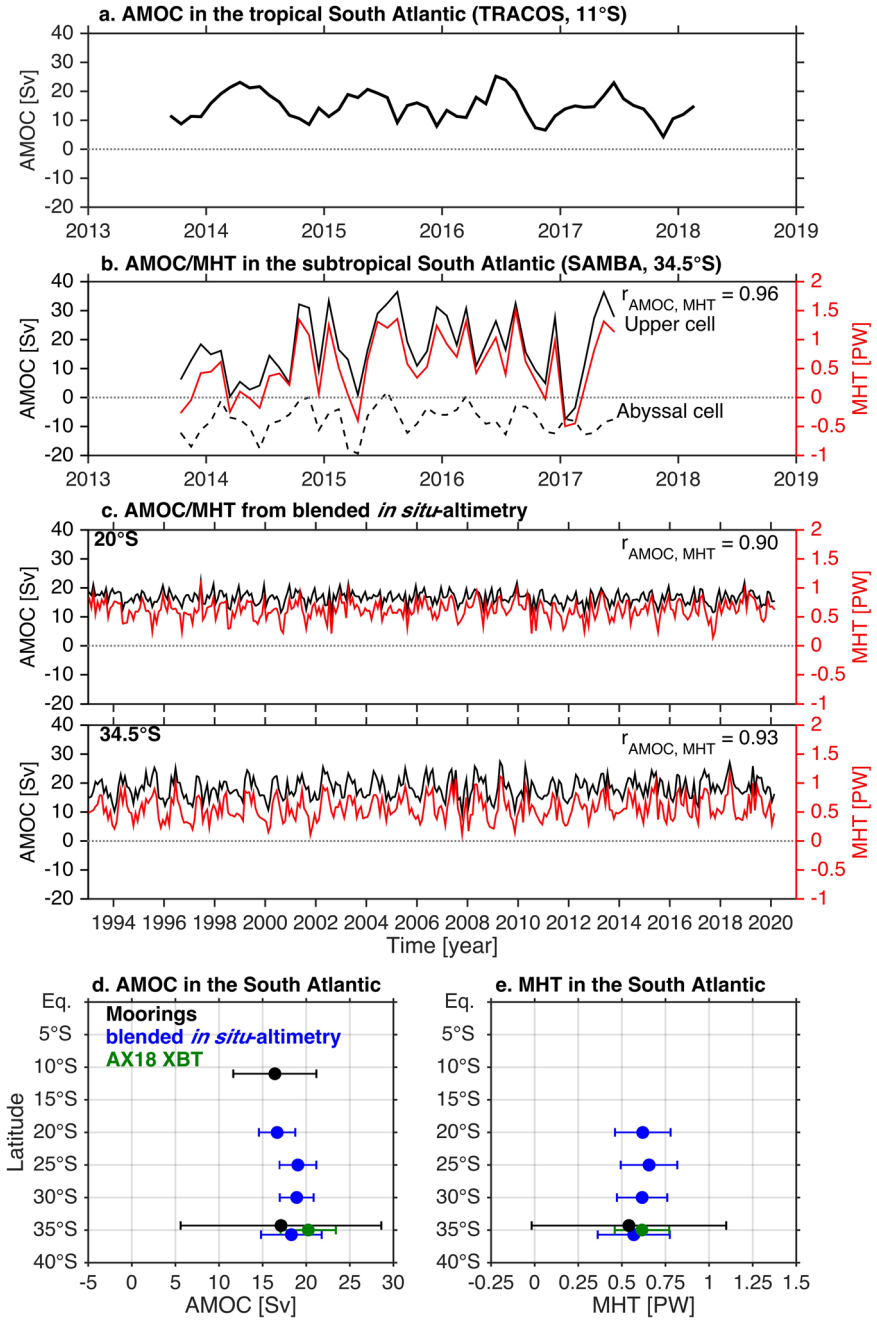

Fig. 4 Time series of AMOC and MHT in the South Atlantic. Monthly values of AMOC upper cell transport (black solid curves) and MHT (red curves, when available) time series from mooring observing arrays: **a** TRACOS in the Tropical Atlantic[98,115] at 11°S from July 2013 to February 2018, **b** SAMBA in the Subtropical South Atlantic[55,97] at 34.5°S from September 2013 to July 2017. The AMOC abyssal-cell transport below 3000 m at 34.5°S is also shown[97] (black dashed curve). **c** Monthly AMOC upper cell transport and MHT time series constructed from blended products based on combinations of in situ hydrographic profiles and satellite altimetry[57] at two selected latitudes in the South Atlantic (20°S and 34.5°S) during 1993–2020. The correlation values between AMOC and MHT ($r_{AMOC,MHT}$) time series are included when available. **d**, **e** Temporal mean (circles) ± one standard deviation (horizontal error bars) of the available monthly AMOC and MHT full-length records, respectively, from moorings[55,97,98,115] (black) and blended in situ altimetry products[57] (blue), and from the AX18 XBT quarterly repeated transect[57] during 2002–2019 (dark green), as a function of latitude. Positive values indicate northward transport, and negative values indicate southward transport. AMOC Atlantic Meridional Overturning Circulation, MHT Meridional Heat Transport.

two arrays is comparable[97,98]. The ~30-year AMOC and MHT records produced from the blended in situ and satellite observations show that the relative importance of the geostrophic and Ekman components driving AMOC and MHT fluctuations vary with both time-scale and latitude between 20 and 34.5°S[57,165]. This suggests that different mechanisms (wind forcing, buoyancy forcing, and internal ocean dynamics) are responsible for driving the observed fluctuations at different latitudes. A well-defined AMOC and MHT seasonal cycle was found between 20 and 34.5°S, with the largest amplitudes (4 Sv and 0.3 PW, respectively) at 34.5°S[57,165]. While these records indicate that there is no MHT coherence between the South and North Atlantic on interannual time-scales, northward propagation of large MHT anomalies from 34.5 to 20°S with a 9-month lead time were found, thus

expanding our understanding of the latitudinal connectivity of the AMOC system[57]. It is plausible that MHT variations on interannual and shorter time-scales are dominated by regional processes with low coherence across the gyres and hemispheres, as has been suggested by numerical simulations[176]. Longer observational records will improve analyses of AMOC/MHT meridional coherence within the Atlantic basin on seasonal, interannual, decadal, and longer time-scales and across a range of processes.

On shorter time-scales ranging from a few days to weeks, moored observations from TRACOS (11°S) and SAMBA (34.5°S) have also revealed large amplitudes of variability and rapid changes of the boundary current transports by the NBC/NBUC, the BC, and the DWBC near the western boundary[113,122,177] and by the Angola Current, BCS, and Deep Eastern Boundary Current (DEBC) near the eastern boundary[85,178,179]. These results highlight the strength of continuous observing systems to resolve these highly variable flows near the continental slope, which in turn are key contributors to the upper and abyssal AMOC transports variability across the basin.

Moored instruments and regular hydrographic sections provide unprecedented temperature, salinity, velocity and/or bottom pressure information near the western and eastern boundaries of the South Atlantic[74,84,85,98,113,114,122,177–181]. However, observations from which meridional heat or freshwater transports can be computed in the interior of the basin are still very sparse. A new technique for estimating interior full-depth temperature profiles by combining satellite, CTD, and Argo profile measurements determined an average MHT during 2013–2017 of 0.5 PW, with a daily standard deviation of 0.8 PW, for the SAMBA array at 34.5°S[55]. This time-mean estimate falls within the range of the previous results from snapshot shipboard measurements and blended products (Table 2) and demonstrates that moored arrays on the boundary combined with ancillary data in the interior can be used to continuously observe heat transport.

Regardless of the observational platform, studies consistently show that the upper cell AMOC volume and heat transports vary in a coherent manner (i.e., the AMOC and MHT time series are strongly correlated with one another with significant correlation coefficients r greater than 0.7 (Table 2; Fig. 4b, c). Furthermore, the characteristics of their variability are very similar on intra-seasonal, seasonal, and interannual time-scales. Linear regressions of AMOC volume and heat transport find that a + 1 Sv change in AMOC at 34.5°S is equivalent to approximately a + 0.05 PW increase in MHT[55,182].

From SAMBA, the AMOC upper cell and MHT appear to be strengthening during 2013–2017 by 2.5 ± 3.8 Sv year^{-1} and at a rate of 0.14 ± 0.18 PW year^{-1}, respectively[55]. These short-term trends, while large, are not statistically significant relative to the large interannual modulation observed during this 4-year time period at 34.5°S. However, other studies suggest significantly smaller trends in transport when a longer time period is considered. For example, significant positive AMOC upper cell transport trends are observed from 1993 to 2020 at 25°S and 34.5°S (0.44 ± 0.38 Sv decade^{-1} and 0.48 ± 0.36 Sv decade^{-1}, respectively), while a significant MHT trend is detected only at 34.5°S (0.03 ± 0.01 PW decade^{-1}) from the blended in situ and satellite altimetry data[57] (Fig. 4c). More years of continuous measurements are likely necessary to detect significant longer period signals and trends in the moored transport records given the large variability on short time-scales (e.g., Fig. 4b).

Cross-comparisons of the in situ/satellite AMOC/MHT estimates with that from moored arrays indicate that while the time means agree well, they usually yield low correlations and different seasonal-to-interannual variability even after subsampling the daily mooring records at monthly resolution[57,183] (Fig. 4b–e). The lack of coherence suggests that the estimates are sensitive to the methodology and/or sampling characteristics of the observations used to derive them. While the CTD, XBT and blended records have unquestionably expanded our understanding of the oceanic fluxes across multiple latitudes, the lower temporal sampling rates from synoptic (snapshot) observations and/or monthly gridded products (which combine observations with different temporal resolutions) may miss the high-frequency AMOC and MHT fluctuations captured by the mooring arrays. Moreover, moored arrays that use bottom pressure information to provide information about the barotropic contribution produce more energetic AMOC and MHT time series[15,55,97] than the other observational methods that use an assumption of net-zero volume (mass) transport (Box 1). To better determine the state of the AMOC/MHT and understand its variability, it is necessary to understand the physical reasons for these observational disparities (taking into account the uncertainties associated with each technique) when longer time series from all of these observing systems become available.

Estimates of the meridional freshwater transport by the overturning circulation, computed either from the sea surface to the seafloor or from the sea surface to the base of the upper AMOC cell (nominally 3000 dbar), have been limited to full-depth CTD sections[56,166–168], XBT transects[16], and inverse models[61,184,185]. Most trans-basin observations collected to date have shown that the freshwater transport associated with the overturning circulation (M_{ov}) between 11°S and 34.5°S is southward[16,166,167,184], and may have increased in strength over the past 30 years associated with increasing salinity trends in the upper ocean[184] (Fig. 3c). In contrast, a recent study found northward M_{ov} from a 2017 trans-basin section along 34.5°S[56]. As mentioned earlier, the sign (i.e., direction) of the freshwater transport by the AMOC upper cell at this latitude may control whether AMOC exists in a bistable or monostable state, with far-reaching climate implications. Given their importance, more M_{ov} estimates from observations are clearly needed. Continuous M_{ov} estimates from the RAPID/MOCHA/WBTS array in the subtropical North Atlantic (26.5°N; Fig. 1; Box 1) and Argo data suggest that a linear relationship describing 91% of the variance exists between AMOC and M_{ov}[186] and so a + 1 Sv increase in AMOC volume transport at 26.5°N is roughly equivalent to a −0.05 Sv decrease in M_{ov}. Thus it seems feasible that future blended in situ and satellite products and moored observations can be used to construct M_{ov} time series similar to approaches used for MHT[55,57,164,165].

Dynamic inflows to the overturning circulation in the South Atlantic from the South Pacific and Indian basins

In the South Atlantic, branches of the AMOC are carried by currents at the western and eastern boundaries of the basin[6,65,69,119] (Fig. 1). In the west, cold fresh waters carried by the MC, a branch of the ACC, enter the basin through Drake Passage to flow northward along the coast of South America and then turn eastward as they encounter the warm salty southward flowing BC. Together, these waters flow eastward and join the warm water masses in the BCS, entering via the Agulhas Leakage, to flow northward off South Africa and Namibia. Both of these water mass routes feed the SEC, which crosses the South Atlantic south-east to north-west. Ultimately, these waters reach the equatorial regions, feeding into the NBC.

The Antarctic Circumpolar Current in Drake Passage. As well as influencing Atlantic circulation, the ACC transport through Drake Passage serves as a valuable metric for validating ocean and climate models and constraining inverse models. Few numbers have been more cited for this reason than the estimate of 134 Sv

of time-mean ACC transport from the International Southern Ocean Studies (ISOS) program conducted in the 1970s[187,188]. However, a reassessment of the ISOS data estimated the uncertainty of that mean ACC transport as 27 Sv[189]. Recent observational estimates of the total ACC transport using different methodologies can differ by more than 30 Sv, with 141 Sv estimated from the DRAKE experiment[190], 173 Sv estimated from the cDrake experiment[191,192], and 175 Sv determined from an analysis of Argo float displacements and historical hydrography[193]. The attribution of the differences between the Drake Passage observational estimates is primarily due to differences in the estimates of the barotropic component of the ACC transport[102,192].

Recent high-resolution global numerical simulations are providing useful context in interpreting these observational transport estimates. A multi-decadal global ocean and sea-ice simulation based on the HYbrid Coordinate Ocean Model (HYCOM)[194] with 1/12° horizontal resolution was analyzed to diagnose differences between the DRAKE and cDrake transport estimates[102]. The total time-mean HYCOM-modeled transport was 157 Sv which falls between the DRAKE and cDrake estimates, and also closely agrees with estimates from other recent data-constrained models (e.g., 155 Sv;[195] 149 Sv[196]). In general, good agreement between the model and observations is found for the baroclinic component of transport; the HYCOM estimates[102] (Fig. 5a) track the 20-year time series of baroclinic transport estimated from annually repeated GO-SHIP hydrographic sections along SR1b[197]. The daily continuous observational estimates from cDrake permit the study of the variability of the full-depth ACC baroclinic transport in detail[191]. The energetic baroclinic transport had a standard deviation of 8.1 Sv with 65% of the transport variance concentrated at periods shorter than 60 days, highlighting the high-frequency variability in the record, while the annual means were steady during 2007–2011[191] (magenta curve in Fig. 5a). The contemporaneous five samples of baroclinic components from SR1b and cDrake agree well[191] (black dots and magenta curve in Fig. 5a). The main challenge for observations appears to be the barotropic component, which requires accurate velocity measurements across the entire passage at high spatial resolution. Shipboard ADCP (SADCP) measurements, although limited to the upper 1000 m, provide direct velocity measurements at the required horizontal resolution, on the order of 5 km[198]. The time-mean ACC transport in the upper 1000 m estimated from repeat SADCP transects of Drake Passage is 95 Sv[198], in agreement with the 93 Sv estimated from HYCOM in the upper 1000 m (Fig. 5c). Finally, although the structure and strength of winds over the Southern Ocean have been changing over the past several decades[199,200], there is at present little evidence of a significant trend in the recent ACC transport estimates, and no long-term trend was found in the HYCOM Drake Passage transport over 40 years[102].

While the ACC transport has remained steady, trends in ACC eddy energy appear to be correlated with interannual and longer time-scale changes in the prevailing winds[201,202]. This phenomenon, predicted by theory and observed in eddy-permitting models, is termed eddy saturation, whereby increased winds result in increased eddy kinetic energy rather than increased circumpolar transport[203]. A related phenomenon for the meridional overturning circulation is eddy compensation, whereby poleward eddy fluxes compensate for increases in the equatorward wind-driven component of overturning transport[202]. Thus, poleward eddy fluxes are a key dynamical process for closing the AMOC in the Southern Ocean. Drake Passage is one of the few polar regions where simultaneous measurements of temperature and velocity have made it possible to estimate eddy heat fluxes. Moored observations during the ISOS program yielded consistently poleward eddy heat fluxes, although estimates varied with depth and location and were also sensitive to time series length[204,205]. Longer time series from the recent cDrake experiment[206] provided eddy heat flux estimates that were statistically stable over 2-year subsets. These fluxes were predominantly poleward, with 50% of the heat flux surface intensified above 1000 m and uniformly distributed below[207]. The strongest heat fluxes observed by cDrake were between the Subantarctic and Polar Fronts, but the 50 km spacing in southern Drake Passage may not have captured the full eddy heat flux of the narrow Southern ACC Front. The high horizontal resolution is required in southern Drake Passage where the radius of deformation is of the order of 15 km. Using seven years of high-resolution SADCP and AX25 XBT temperature data from spatially near-repeated underway surveys in Drake Passage (Box 1; Box 2), poleward and surface-intensified eddy heat fluxes were identified not only in the surface layer of the Polar Front but also in the Southern ACC Front[208]. These results were recently updated using the now 20-year-long time series, calculating both time-mean and time-varying streamlines to isolate the dynamically important across-ACC heat flux component[209]. The time-varying streamlines provide the best estimate of the across-ACC component because they track the shifting and meandering of the ACC fronts. The depth-integrated (0–900 m) across-stream eddy heat flux is poleward and maximum in the south flank of the Subantarctic Front -0.10 ± 0.05 GW m^{-1} (1 GW equals 10^{-6} PW) and decreases to become statistically insignificant toward the south. The long time series provides an uncommon opportunity to explore the seasonal cycle of eddy heat flux. The poleward eddy heat flux in the Polar Front Zone is enhanced during austral autumn–winter, suggesting a seasonal variation in eddy-driven upwelling and thus the overturning circulation[209].

Agulhas Leakage in the Cape Basin. An interocean exchange route that is fundamental for the AMOC lies in the gap between the southern shores of Africa and the ACC. Lagrangian experiments using eddy-resolving ocean and, more recently, climate, models are able to quantify the simulated Agulhas Leakage from the Indian Ocean and allow estimates of associated water mass properties and their transformation[62,65,67,81,119,210]. In the real ocean, however, Agulhas Leakage waters are difficult to trace and the interocean fluxes, which occur as eddies and filaments spun off the Agulhas retroflection, represent an extreme challenge to quantify because of the highly energetic environment[131,211–214].

Recently, it has been possible to disentangle some elements of the Agulhas Leakage complexity using eastern boundary observations from the SAMBA observing system[85] (Box 1). While the total Agulhas Leakage is estimated to range from ~5–15 Sv[132] to 21.3 ± 4.7 Sv[215], the SAMBA observations quantify a time-mean northward transport of thermocline waters across 34.5°S within the Cape Basin of 24 Sv with the large variance (standard deviation of 17 Sv) due to the passing of Agulhas Rings[85]. This transport is associated with the upper limb of the AMOC and contributes to the northward transport of heat and salt (Fig. 1). The SAMBA observations demonstrate that water mass exchange in the Cape Basin occurs primarily through advection by mesoscale eddies and via broad water mass intrusions brought about by intense dipoles[84]. Importantly, the study also highlights the need to continuously sample the full water column, as inter-basin exchanges occur intermittently and can affect the buoyancy and currents at multiple depths and time-scales.

Agulhas Rings act as the loci of intense water masses transformations; large amounts of Indian Ocean central waters captured in the ring cores are transformed into subtropical mode

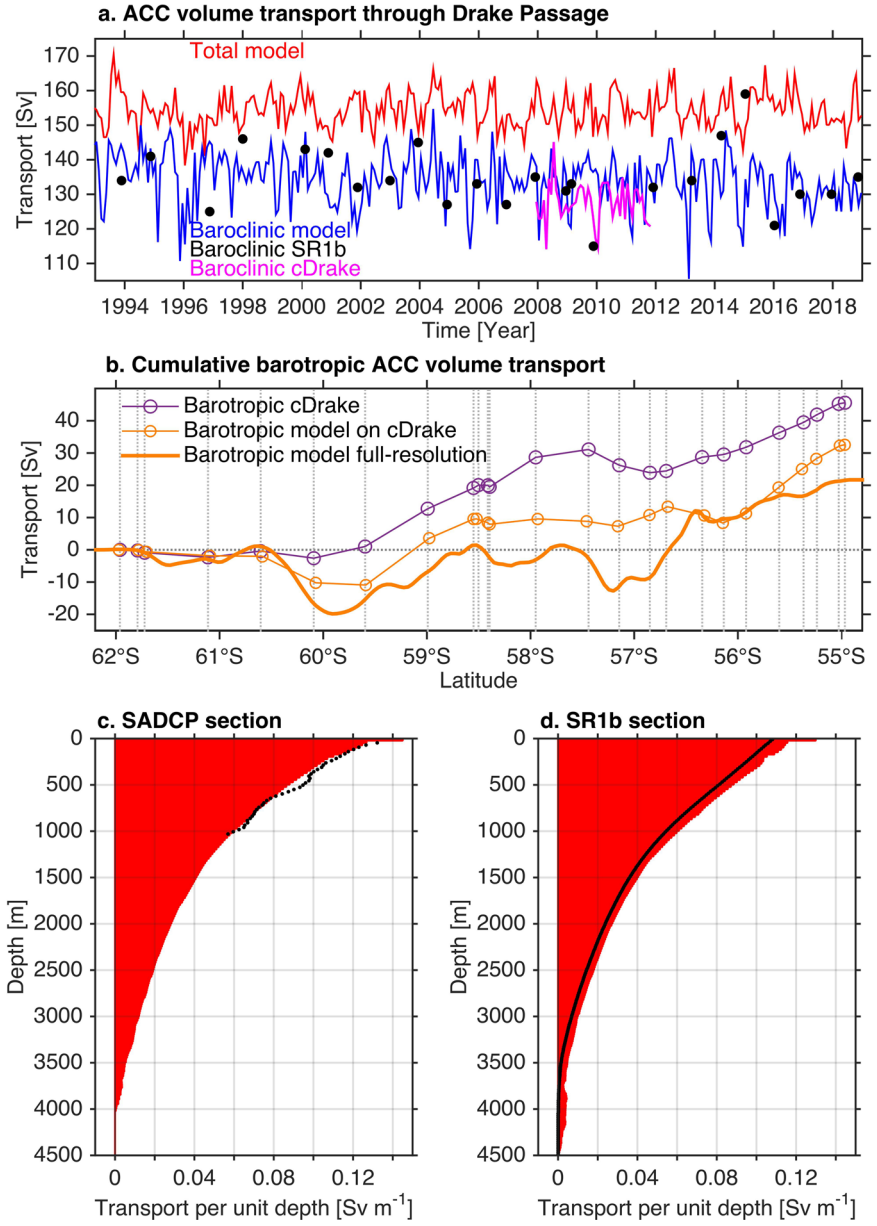

Fig. 5 Volume transport through Drake Passage. a Monthly values of total (red curve) and baroclinic (blue curve) transports across the repeat SR1b hydrographic section in Drake Passage computed from the HYbrid Coordinate Ocean Model (HYCOM) in comparison with baroclinic transport estimated from 24 SR1b hydrographic surveys[102] (black circles) over 1993–2018 and with monthly baroclinic transport (magenta curve) estimated from the continuous cDrake observations[191] from December 2007 to October 2011. The HYCOM transports (available between 1979–2020) are shown for the period 1993–2018 (coincident with the 24 SR1b observations). **b** Cumulative barotropic Antarctic Circumpolar Current (ACC) transports from south to north across Drake Passage[102]. The circled purple line is the cumulative barotropic transport based on cDrake observations[192]; the circled and thick orange lines are the HYCOM-modeled cumulative barotropic transports calculated using velocities subsampled at the cDrake mooring locations and at the full model resolution, respectively. The dashed vertical lines and circles indicate the cDrake mooring locations. **c**, **d** Vertical profile of transport per unit depth as a function of depth at the Drake Passage repeat SADCP section and repeat hydrographic SR1b section from HYCOM and observations[102]. The red horizontal bars are the HYCOM-modeled total transport. In **c**, the black circles are SADCP observations[198]. In **d**, the black circles are baroclinic transports based on the long-term SR1b hydrographic surveys. Positive transports correspond to eastward flow.

waters across a relatively large temperature range[128,216]. Earlier transport estimates of 2–10 Sv have been made by observing long-lived Agulhas Rings from ships or satellites[59,217–222]. However, simulations consistently underestimate the amount of leakage that is carried in the rings and it is mostly the non-eddy part of the flux that plays the dominant role in the modeled Agulhas Leakage transport[210,223,224]. This is most likely because the models do not adequately represent the full spectrum of meso- and submeso-scale (less than 50 km) variability, hence biasing their estimates low and introducing large uncertainty into the estimates. Recent studies that combine satellite altimetry with in situ hydrographic data have enabled a better assessment of the impact of Agulhas Rings in efficiently connecting the eastern and western boundary systems of the South Atlantic[216,222,225,226]. Despite the complex dynamics associated with the passage of the Agulhas Rings (with many splitting and merging in the Cape Basin) some rings remain as coherent subsurface structures while crossing the South Atlantic, taking about three years to reach the

other side of the basin on average[216,222,225,226]. There is potential for observations of the Agulhas Current in the Indian Ocean to shed light on leakage variability that is thought to be driven by the upstream control of leakage by wind and meanders[227], although recently, these controls have come into question[228,229].

The SAMBA array has also led to a better assessment of the underlying time-mean southward transport of −12 Sv (standard deviation of 17 Sv) associated with the DEBC in the South Atlantic[85]. This deep current includes the southward flow of an eastern vein of NADW[64,77,78,230]. The SAMBA observations further indicate that much of the DEBC must recirculate within the Cape Basin, with a smaller portion of the flow participating in the global overturning circulation[85].

Applications for SAMOC observations for improved ocean and climate models used for weather and climate forecasts

The considerable expansion of the in situ SAMOC observational network over the past 15+ years (Box 1), particularly along the SAMBA line at 34.5°S and the TRACOS line at 11°S, have provided unprecedented information about the structure and variability of the AMOC transports at these two latitudes. However, continuous in situ observational AMOC records are still limited in space and time, and models are needed to study AMOC mechanisms and the impact of AMOC on weather and climate. Model-based studies[30,32,103,104,125,231,232] have provided important insights into AMOC behavior and impacts in the South Atlantic, but the value of those insights depends on the fidelity of the models to the real ocean. In order to assess the climate impact of the AMOC and predict future variability, it is critical that climate models used for weather and climate forecasts accurately simulate the sensitivity of the AMOC in the South Atlantic in response to forcing.

Observations from both the North and South Atlantic Ocean suggest that the geostrophic contribution to the volume and heat transports of the AMOC plays an equal or greater role compared to that played by the wind-driven Ekman transport in terms of the total AMOC and MHT seasonal to interannual variability[13,26,57,153,174,233,234]. However, studies based on earlier eddy-permitting (¼° to 1° horizontal resolution) numerical models[235–238] indicated that the seasonal to interannual variations in the modeled AMOC and MHT are predominantly controlled by the Ekman transport. The AMOC estimates at 34.5°S from monthly climatologies of temperature and salinity constructed from observations and numerical models suggested that the seasonality of the geostrophic transport from observations is largely controlled by density variations at the western boundary, but in the models, the eastern boundary dominates due to poor representation of the MC strength at the western boundary[239]. The weak seasonal cycle in the modeled geostrophic transport was primarily attributed to excessively strong baroclinicity below the surface mixed layer, whereas the observations show a strong vertical coherence in the velocity down to 1200 m.

Another well-known disagreement between observations and models is the direction of the freshwater transport induced by the overturning circulation (M_{ov}) near the southern boundary of the Atlantic[16,90,91,120,166,167]. Contrary to the positive values of the M_{ov} from numerical models[35,50,240–242], most recent observation-based estimates of the M_{ov} in the South Atlantic[16,120,166,167,184] gave negative values ranging from −0.28 to −0.05 Sv (with the exception of the recent snapshot estimate from a trans-basin cruise at 34.5°S[56]), suggesting that changes in the AMOC would amplify the freshwater anomalies in the convection sites. As a result, contrary to the monostable state of the AMOC from models, observations suggest that the AMOC is bistable and might collapse with a large enough freshwater perturbation. The model-data difference in freshwater transports has been attributed to the biases in the modeled salinity fields: too fresh in the northward-flowing upper layer and too salty in the southward flowing lower layer[35,50,91,240–242].

Eddies play an important role in transporting heat and freshwater in the South Atlantic, and improved eddy parameterizations and/or higher resolution numerical models are required to properly simulate eddy characteristics and their impacts on regional and global climate[66,201,243]. A recent study to investigate the impact of model resolution on the subtropical South Atlantic variability demonstrated the dominant role geostrophic transport plays in controlling the MHT variability in an eddy-resolving (0.1° horizontal resolution) simulation while both the geostrophic and Ekman transports influence MHT variability in a non-eddy resolving (1° horizontal resolution) simulation[244]. Interestingly, while model MHT at the northern boundary of the South Atlantic (8°S) drives heat content variability in the non-eddy-resolving simulation, in the eddy-resolving simulation ocean heat content variability is predominantly driven by MHT at the southern boundary of the South Atlantic (35°S). Recently, a 1/20° horizontal resolution ocean model was compared to AMOC observations at multiple latitudes in the North and South Atlantic, and was able to reproduce well the AMOC volume transport variations at 34.5°S and AMOC, NBUC, and DWBC transport variations at 11°S[104]. Thus, better agreement between models and observations may be found as more models move towards eddy-resolving horizontal resolution.

The increased observations in the last 15+ years in the South Atlantic are invaluable for use in the initialization, validation, and evaluation of newer generations of ocean general circulation and coupled climate models[103,104]. Models can provide information on multi-decadal to millennial time scales; however, the differences in the AMOC volume, heat and freshwater transports between numerical models and observations suggest that the AMOC variations in models respond differently to forcing than in the real ocean. It is challenging to implement model improvements based on comparatively short observational records. Thus, existing model-data differences point once again to the need for longer-term measurements in the South Atlantic from moorings to better assess the realism and representation of processes that control AMOC strength and variability in numerical models.

Summary and future perspectives

Through its long-term storage and transport of heat, freshwater, and carbon, ocean circulation strongly influences the magnitude, pace, and regional impacts of anthropogenic climate change. These processes are of particular importance in the South Atlantic Ocean, as they influence, and are influenced by, AMOC variability, the development of key water masses, and interocean exchanges. This review provides a comprehensive overview of recent advances in understanding AMOC variability in the South Atlantic, enabled by the tremendous growth of the SAMOC observing system since its inception in 2007.

As a result of the excess heat absorbed from the atmosphere associated with ongoing planetary warming, AMOC variability, interocean exchanges from the Pacific and Indian basins, and other factors elucidated in this review, the South Atlantic Ocean has warmed from the surface to the deep and abyssal ocean[12,75,76,147,148,151,163] (Fig. 3a, b, e). Upper ocean South Atlantic salinity has increased, while intermediate, deep, and abyssal water masses are freshening[148,151,158] (Fig. 3c, d). Recent observational and modeling evidence suggests that a reduction in the strength of the AMOC associated with anthropogenic warming is linked to additional surface South Atlantic warming

and salinification[135,136]. Continuing to monitor these water mass changes and their causes is an ongoing priority for South Atlantic research.

Tracking water masses and their changes by combining models and observations has allowed us to refine our understanding of AMOC pathways in the South Atlantic. Quantifying the relative contributions of interocean exchanges from the Indian and Pacific basins into the South Atlantic, allows for a better understanding of the warming and salinification trends observed in upper layers[65,81,122,137] (Fig. 3a, c). Observational evidence of NADW in the DEBC[85] and in the interior[64,77,78,230] in the South Atlantic has elucidated new deep water mass pathways. However, many open questions about AMOC water mass pathways remain, particularly the zonal interior paths, and the pathways between the well-observed latitudes. The South Atlantic Gateway Array (SAGA) array deployed along 10°W in 2021 measures the zonal flows carried by the BCS and Agulhas Rings and the underlying NADW interior pathway from the west to east in the mid-latitude central South Atlantic (Box 1) and will help to answer some of these questions in the near future.

The AMOC arrays have expanded over time to include more moorings to better resolve boundary current processes associated with the AMOC variability, such as wind and buoyancy forcing, advection, and/or wave propagation[85,113,122]. Even the relatively short trans-basin mooring records available to date have transformed our understanding of the energetic South Atlantic circulation, its dynamics, and its contribution to upper and abyssal AMOC variability on daily to interannual time scales[15,97,98], illustrating the need for high-frequency measurements to avoid aliasing rapid short time scale signals. The dominant mechanisms causing changes in the AMOC strength varies between wind forcing, buoyancy forcing, and internal ocean dynamics on seasonal, interannual, and decadal time scales between 11°S and 34.5°S[15,57,97,98] (Fig. 4; Table 2). Because upper cell AMOC and MHT vary in a consistent manner[16,55,57,97] (Fig. 4b, c), changes in AMOC can impact ocean heat content, pointing to the importance of sustained AMOC monitoring at various latitudes in the South and North Atlantic.

The AMOC volume and property (e.g., heat) transports appear to be somewhat sensitive to the methodology, assumptions, and/or sampling characteristics of the observations used to derive them. For example, the phasing (semi-annual vs. annual) and amplitude of the seasonal cycles currently vary between different studies using moored arrays or blended in situ and satellite measurements at the same latitude, with moored arrays producing records with larger transport variations than other methods. It is possible that the temporal lengths of some of the observational records are still too short to produce directly comparable estimates and/or ascertain whether any of the observing systems miss or alias important contributions to the AMOC transport variability. Future research plans include reconciling the different estimation methods when longer overlapping time series become available. It is important to acknowledge that while infrequent or monthly proxy or partial-basin observations will never be as accurate as full-depth trans-basin continuous moored measurements, these observations are cost-effective and available on a longer time-scale and at a wider range of locations, thus providing high scientific value despite the inherent limitations.

The observing systems at the gateways from the Pacific and Indian basins monitor interocean exchange processes such as buoyancy exchange, winter mixing, convection, and upwelling. Estimates of the total ACC transport through Drake Passage from a number of recent targeted field campaigns show higher ACC transports (141–173 Sv) than historical values, with increased transport largely due to improved estimation of the barotropic component of the flow[191,192]. The annual mean ACC transport appears to have been steady from observations[191,192], and no long-term trend has been detected evaluating ACC transport in a data-constrained model[102]. Maintaining long-term observations of the ACC barotropic component remains a challenge (e.g., the highly-resolved cDrake experiment ended in 2011), making it hard to directly and continuously monitor the total ACC transport. Thus, it becomes important to have realistic data-constrained models of ACC transport and to continue monitoring via the annual full-depth SR1b hydrographic cruises and repeat XBT/SADCP transects. In addition, observations and models suggest that the baroclinic and barotropic ACC transports are not correlated; therefore, monitoring either transport component alone seems insufficient to assess the temporal variability of the total ACC transport[102].

In comparison to Pacific-Atlantic, Indo-Atlantic ocean exchanges are less well observed because they occur intermittently since they are largely accomplished through eddies and/or filaments[84]. The eastern SAMBA moorings measure highly variable northward transports of thermocline waters at 34.5°S, associated with the passage of Agulhas Rings that contributes to transports by the upper limb of the AMOC. Developing the techniques and methods to better estimate the eddy flux contributions to interocean exchange, and hence reconcile the disparate estimates of transport by the Agulhas Rings[85,132,215] remains an ongoing challenge. As a step in this direction, the number of eastern SAMBA PIES moorings was doubled in 2021 from five to ten sites between Walvis Ridge and the African coast in order to better resolve the variability associated with the Agulhas Leakage into the South Atlantic.

Topographically constrained narrow boundary current flows and mesoscale features and processes associated with eddies are often inadequately represented in low-resolution numerical models, which can lead to an inadequate representation of the AMOC. SAMOC observations in the past 15+ years have provided unprecedented information about the structure and variability of the AMOC and water mass distributions and pathways, which are invaluable for validating and constraining models[65,103,104,234]. Model-data intercomparisons are helping to reconcile differences in key processes driving the AMOC in the South Atlantic, such as the role of eddies, AMOC pathways, the relative roles of geostrophic and wind-driven Ekman transports in setting AMOC variability, and the direction of the meridional freshwater transports. Recently, an ocean model with more realistic atmospheric forcing and eddy-resolving horizontal resolution was able to better reproduce the observed AMOC volume transport variations at 11°S and at 34.5°S, indicating the need for models with better representation of boundary flows over sloping topography and mesoscale eddies to accurately represent AMOC variability in the South Atlantic[104].

Continuous evaluation and improvements of the existing observing systems are essential for further scientific advances. For example, three additional moored instruments in the interior of the basin were added to the SAMBA array in 2019–2021 to further improve estimates of the interior and abyssal flows. Future plans include extending the western and eastern SAMBA measurements to the shelf-break regions to better observe processes at the continental boundaries, where boundary currents intensify, and to better constrain basin-wide AMOC estimates. At the western edge of SAMBA in the Southwestern Atlantic two tall dynamic height moorings will be deployed in 2022 at the continental shelf break and at the base of the continental slope to add observations of the vertical structure of the BC and of the DWBC, respectively. Similarly, the eastern SAMBA array will soon include additional moorings on the South African shelf.

Most continuous observing systems in the South Atlantic have focused on measuring physical properties (velocity, temperature, and salinity) to determine volume and heat transports.

More time series estimates of AMOC freshwater transport are needed to determine whether volume and freshwater transport co-vary, and whether or not observed freshwater transports are consistently positive or negative, suggesting AMOC is monostable or bistable, respectively. Given the important role of the AMOC in modulating carbon uptake by the ocean from the atmosphere, future moored array improvements could include new biogeochemical sensors, which would allow for the estimation of oceanic nutrients and carbon fluxes. Some of the South Atlantic arrays are starting to incorporate dissolved oxygen sensors (e.g., some TRACOS and SAMBA moorings) to better track water masses and to study combined biogeochemical and physical properties changes relevant for marine ecosystems.

In addition to augmenting the measurements made by existing platforms, it is important to develop pilot observing systems to study AMOC-related processes in undersampled regions and shed light on other remaining unknowns. Such observational arrays could also include surveying from newer autonomous underwater vehicles and uncrewed surface vehicles. Pilot and process studies like the SAGA program can help to increase our understanding of the zonal component of the AMOC, and deploying more bottom-mounted moorings and deep Argo floats in the South Atlantic is important for quantifying ongoing deep and abyssal temperature and salinity changes. Expendable data pod technology systems are being tested at a few SAMBA and SAGA mooring sites to more routinely (once or twice a year) collect data recorded by bottom-mounted moorings, reducing ship time requirements and lowering the risk of data loss.

Pan-Atlantic observational efforts are crucial for improving climate models and tracking the projected decline of AMOC in the next century in response to anthropogenic forcing[19,41]. Sustained and continuous monitoring of AMOC changes in the South Atlantic is needed to assess their impacts on climate patterns, such as shifts in regional surface temperature and precipitation patterns[32] and extreme events (e.g., marine heat waves, hurricanes), the variability of the key boundary current systems[85,113,122,177], coastal sea level rise, warming/cooling or salinification/freshening of the ocean[75,76], deoxygenation and acidification processes. All of these phenomena have large societally-relevant planetary impacts on agriculture, fisheries, infrastructure, and health around the globe[103,245].

Sufficiently long in situ AMOC time series in the North and South Atlantic, together with high-resolution numerical models, will enable a synthesis of the observed transports to elucidate how each key component contributes to the AMOC's mean state and variability, the forcing processes, the influence of meridional freshwater transport on AMOC stability, and the mechanisms responsible for the meridional coherence and propagation/pathways of AMOC signals on multi-decadal time scales. These studies require international coordination, collaboration, and data and code sharing among scientists within the entire Atlantic Ocean basin.

The SAMOC initiative is the result of a concerted international effort where observing components are combined towards a common objective taking advantage of the available resources. Sustaining a long-term AMOC observing system in the South Atlantic for decades will be challenging but is necessary to address the many outstanding research questions. The ability to maintain these observing systems in the South Atlantic depends not just on institutions and funding agencies in many countries, but also on the availability of resources (research infrastructure, trained personnel). Reducing the costs of these observing programs by determining which sites are key for sustained monitoring, and reducing the need for ship time to collect data from the moorings (i.e., through technological innovations), are high priorities for all of the ongoing AMOC arrays. The SAMOC observing system can learn from assessments ongoing in the North Atlantic[96], but must be mindful that a "one-size-fits-all" AMOC observing strategy may not be possible because of the many unique features of the South Atlantic that have been highlighted in this review.

Data availability

The datasets analyzed in this review are cited in the appropriate sections of the manuscript text. Data from the South Atlantic MOC Basin-wide Array (SAMBA) can be found at: https://www.aoml.noaa.gov/phod/SAMOC_international/samoc_data.php. The gridded Argo climatology[246] used in this study is freely available (https://sio-argo.ucsd.edu/RG_Climatology.html). The Argo data were collected and made freely available by the International Argo Program and the national programs that contribute to it (http://www.argo.ucsd.edu, http://argo.jcommops.org). The Argo Program is part of the Global Ocean Observing System.

Received: 23 May 2022; Accepted: 23 November 2022;
Published online: 19 January 2023

References

1. Trenberth, K. E. & Caron, J. M. Estimates of meridional atmosphere and ocean heat transports. *J. Clim.* **14**, 3433–3443 (2001).
2. Trenberth, K. E., Zhang, Y., Fasullo, J. T. & Cheng, L. Observation-based estimates of global and basin ocean meridional heat transport time series. *J. Clim.* **32**, 4567–4583 (2019).
3. von Schuckmann, K. et al. Heat stored in the Earth system: where does the energy go? *Earth Syst. Sci. Data* **12**, 2013–2041 (2020).
4. Stommel, H. The Abyssal Circulation. *Deep Sea Res.* **5**, 80–82 (1958).
5. Broecker, W. S. *The biggest chill: when ocean currents shifted, Europe suddenly got cold; could it happen again?* (American Museum of Natural History, 1987).
6. Rintoul, S. R. South Atlantic interbasin exchange. *J. Geophys. Res.* **96**, 2675–2692 (1991).
7. Talley, L. D. Shallow, intermediate, and deep overturning components of the global heat budget. *J. Phys. Oceanogr.* **33**, 530–560 (2003).
8. Broecker, W. S. The great ocean conveyor. *Oceanography* **4**, 79–89 (1991).
9. Jullion, L., Heywood, K. J., Naveira Garabato, A. C. & Stevens, D. P. Circulation and water mass modification in the Brazil–Malvinas confluence. *J. Phys. Oceanogr.* **40**, 845–864 (2010).
10. Garzoli, S. L. & Matano, R. The South Atlantic and the Atlantic Meridional Overturning Circulation. *Deep Sea Res. Part II* **58**, 1837–1847 (2011).
11. Rimaud, J., Speich, S., Blanke, B. & Grima, N. The exchange of Intermediate Water in the southeast Atlantic: Water mass transformations diagnosed from the Lagrangian analysis of a regional ocean model. *J. Geophys. Res.* **117**, C08034 (2012).
12. Herrford, J., Brandt, P. & Zenk, W. Property changes of deep and bottom waters in the Western Tropical. *Atlantic. Deep Sea Res. Part I* **124**, 103–125 (2017).
13. Kanzow, T. et al. Seasonal variability of the atlantic meridional overturning circulation at 26.5°N. *J. Clim.* **23**, 5678–5698 (2010).
14. Lozier, M. S., Roussenov, V., Reed, M. S. C. & Williams, R. G. Opposing decadal changes for the North Atlantic meridional overturning circulation. *Nat. Geosci.* **3**, 728–734 (2010).
15. Meinen, C. S. et al. Meridional overturning circulation transport variability at 34.5°S during 2009–2017: baroclinic and barotropic flows and the dueling influence of the boundaries. *Geophys. Res. Lett.* **45**, 4180–4188 (2018).
16. Garzoli, S. L., Baringer, M. O., Dong, S., Perez, R. C. & Yao, Q. South Atlantic meridional fluxes. *Deep Sea Res. Part I* **71**, 21–32 (2013).
17. McCarthy, G. D., Haigh, I. D., Hirschi, J. J.-M., Grist, J. P. & Smeed, D. A. Ocean impact on decadal Atlantic climate variability revealed by sea-level observations. *Nature* **521**, 508–510 (2015).
18. Frajka-Williams, E. et al. Compensation between Meridional flow components of the Atlantic MOC at 26°N. *Ocean Sci.* **12**, 481–493 (2016).
19. Frajka-Williams, E. et al. Atlantic Meridional overturning circulation: observed transport and variability. *Front. Mar. Sci.* **6**, 260 (2019).
20. Muir, L. C. & Fedorov, A. V. How the AMOC affects ocean temperatures on decadal to centennial timescales: the North Atlantic versus an interhemispheric seesaw. *Clim. Dyn.* **45**, 151–160 (2015).
21. Buckley, M. W. & Marshall, J. Observations, inferences, and mechanisms of the Atlantic Meridional Overturning Circulation: a review. *Rev. Geophys.* **54**, 5–63 (2016).

22. Caesar, L., McCarthy, G. D., Thornalley, D. J. R., Cahill, N. & Rahmstorf, S. Current Atlantic Meridional Overturning Circulation weakest in last millennium. *Nat. Geosci.* **14**, 118–120 (2021).
23. Jackson, L. C. et al. The evolution of the North Atlantic Meridional Overturning Circulation since 1980. *Nat. Rev. Earth Environ.* **3**, 241–254 (2022).
24. Talley, L. D. Closure of the global overturning circulation through the Indian, Pacific, and Southern Oceans: schematics and transports. *Oceanography* **26**, 80–97 (2013).
25. Hall, M. M. & Bryden, H. L. Direct estimates and mechanisms of ocean heat transport. *Deep Sea Res. Part A* **29**, 339–359 (1982).
26. Johns, W. E. et al. Continuous, array-based estimates of Atlantic Ocean heat transport at 26.5°N. *J. Clim.* **24**, 2429–2449 (2011).
27. Broecker, W. S. Cooling the tropics. *Nature* **376**, 212–213 (1995).
28. Vellinga, M. & Wood, R. A. Global climatic impacts of a collapse of the Atlantic thermohaline circulation. *Clim. Change* **54**, 251–267 (2002).
29. Latif, M., Keenlyside, N. & Bader, J. Tropical sea surface temperature, vertical wind shear, and hurricane development. *Geophys. Res. Lett.* **34**, L01710 (2007).
30. Stouffer, R. J. et al. Investigating the causes of the response of the thermohaline circulation to past and future climate changes. *J. Clim.* **19**, 1365–1387 (2006).
31. Barreiro, M., Fedorov, A., Pacanowski, R. & Philander, S. G. Abrupt climate changes: how freshening of the Northern Atlantic affects the thermohaline and wind-driven oceanic circulations. *Annu. Rev. Earth Planet. Sci.* **36**, 33–58 (2008).
32. Lopez, H., Dong, S., Lee, S.-K. & Campos, E. Remote influence of Interdecadal Pacific Oscillation on the South Atlantic meridional overturning circulation variability. *Geophys. Res. Lett.* **43**, 8250–8258 (2016).
33. Lynch-Stieglitz, J. The Atlantic Meridional overturning circulation and abrupt climate change. *Annu. Rev. Mar. Sci.* **9**, 83–104 (2017).
34. Jackson, L. C. et al. Global and European climate impacts of a slowdown of the AMOC in a high resolution GCM. *Clim. Dyn.* **45**, 3299–3316 (2015).
35. Liu, W., Xie, S.-P., Liu, Z. & Zhu, J. Overlooked possibility of a collapsed Atlantic Meridional Overturning Circulation in warming climate. *Sci. Adv.* **3**, e1601666 (2017).
36. Manabe, S. & Stouffer, R. J. Two stable equilibria of a coupled Ocean-atmosphere model. *J. Clim.* **1**, 841–866 (1988).
37. Intergovernmental Panel on Climate Change (IPCC). *The Ocean and Cryosphere in a Changing Climate: Special Report of the Intergovernmental Panel on Climate Change*. (Cambridge University Press, 2022).
38. Rhein, M. et al. in *Climate Change 2013: The Physical Science Basis. Contribution of Working Group I to the Fifth Assessment Report of the Intergovernmental Panel on Climate Change* (eds. Stocker, T. F. et al.) 255–316 (Cambridge University Press, 2013).
39. Kostov, Y., Armour, K. C. & Marshall, J. Impact of the Atlantic meridional overturning circulation on ocean heat storage and transient climate change. *Geophys. Res. Lett.* **41**, 2108–2116 (2014).
40. Perez, F. F. et al. Meridional overturning circulation conveys fast acidification to the deep Atlantic Ocean. *Nature* **554**, 515–518 (2018).
41. Lee, J.-Y. et al. Future Global Climate: Scenario-Based Projections and Near-Term Information. In *Climate Change 2021: The Physical Science Basis. Contribution of Working Group I to the Sixth Assessment Report of the Intergovernmental Panel on Climate Change*. (ed. Intergovernmental Panel on Climate Change (IPCC)), 553-672 (Cambridge University Press, 2021).
42. Schmittner, A. Decline of the marine ecosystem caused by a reduction in the Atlantic overturning circulation. *Nature* **434**, 628–633 (2005).
43. Kelly, K. A., Drushka, K., Thompson, L., Le Bars, D. & McDonagh, E. L. Impact of slowdown of Atlantic overturning circulation on heat and freshwater transports. *Geophys. Res. Lett.* **43**, 7625–7631 (2016).
44. Lozier, M. S. et al. Overturning in the subpolar North Atlantic Program: A New International Ocean Observing System. *Bull. Am. Meteorol. Soc.* **98**, 737–752 (2017).
45. Palter, J. B., Frölicher, T. L., Paynter, D. & John, J. G. Climate, ocean circulation, and sea level changes under stabilization and overshoot pathways to 1.5 K warming. *Earth Syst. Dynam.* **9**, 817–828 (2018).
46. Caesar, L., Rahmstorf, S., Robinson, A., Feulner, G. & Saba, V. Observed fingerprint of a weakening Atlantic Ocean overturning circulation. *Nature* **556**, 191–196 (2018).
47. IPCC. Summary for Policymakers. in *Climate Change 2021: The Physical Science Basis. Contribution of Working Group I to the Sixth Assessment Report of the Intergovernmental Panel on Climate Change* (eds. Masson-Delmotte, V., P. Zhai, A. Pirani, S.L. Connors et al.) 3–32 (Cambridge University Press, 2021).
48. Broecker, W. S. & Denton, G. H. What drives glacial cycles? *Sci. Am.* **262**, 48–56 (1990).
49. McManus, J. F., Francois, R., Gherardi, J.-M., Keigwin, L. D. & Brown-Leger, S. Collapse and rapid resumption of Atlantic meridional circulation linked to deglacial climate changes. *Nature* **428**, 834–837 (2004).
50. Liu, W., Liu, Z. & Brady, E. C. Why is the AMOC monostable in coupled general circulation models? *J. Clim.* **27**, 2427–2443 (2014).
51. Wüst, G. Schichtung und Zirkulation des Atlantischen Ozeans. Die Stratosphäre. In: *Wissenschaftliche Ergebnisse der Deutschen Atlantischen Expedition auf dem Forschungs-und Vermessungsschiff 'Meteor' 1925–1927* 6, 1st Part, 2, p. 180 (Walter de Gruyter & Co Berlin, 1935). (The Stratosphere of the Atlantic Ocean, ed Emery, W. J., 1978, Amerind, New Delhi, p. 112).
52. Ganachaud, A. & Wunsch, C. Improved estimates of global ocean circulation, heat transport and mixing from hydrographic data. *Nature* **408**, 453–457 (2000).
53. Garzoli, S. L. & Baringer, M. O. Meridional heat transport determined with expandable bathythermographs—Part II: South Atlantic transport. *Deep Sea Res. Part I* **54**, 1402–1420 (2007).
54. Kelly, K. A., Thompson, L. & Lyman, J. The coherence and impact of Meridional Heat transport anomalies in the Atlantic Ocean inferred from observations. *J. Clim.* **27**, 1469–1487 (2014).
55. Kersalé, M. et al. Multi-year estimates of daily heat transport by the Atlantic Meridional overturning circulation at 34.5°S. *J. Geophys. Res. Oceans* **126**, e2020JC016947 (2021).
56. Manta, G. et al. The South Atlantic Meridional Overturning Circulation and Mesoscale Eddies in the First GO-SHIP Section at 34.5°S. *J. Geophys. Res. Oceans* **126**, e2020JC016962 (2021).
57. Dong, S. et al. Synergy of in situ and Satellite Ocean observations in determining Meridional heat transport in the Atlantic Ocean. *J. Geophys. Res. Oceans* **126**, e2020JC017073 (2021).
58. Gordon, A. L. Indian-Atlantic transfer of thermocline water at the agulhas retroflection. *Science* **227**, 1030–1033 (1985).
59. de Ruijter, W. P. M., van Leeuwen, P. J. & Lutjeharms, J. R. E. Generation and evolution of natal pulses: solitary meanders in the agulhas current. *J. Phys. Oceanogr.* **29**, 3043–3055 (1999).
60. Sloyan, B. M. & Rintoul, S. R. Circulation, renewal, and modification of antarctic mode and intermediate water. *J. Phys. Oceanogr.* **31**, 1005–1030 (2001).
61. Lumpkin, R. & Speer, K. Global Ocean Meridional Overturning. *J. Phys. Oceanogr.* **37**, 2550–2562 (2007).
62. Speich, S., Blanke, B. & Cai, W. Atlantic meridional overturning circulation and the Southern Hemisphere supergyre. *Geophys. Res. Lett.* **34**, L23614 (2007).
63. Richardson, P. L. Agulhas leakage into the Atlantic estimated with subsurface floats and surface drifters. *Deep Sea Res. Part I* **54**, 1361–1389 (2007).
64. Garzoli, S. L. et al. The fate of the Deep Western Boundary Current in the South Atlantic. *Deep Sea Res. Part I* **103**, 125–136 (2015).
65. Rühs, S., Schwarzkopf, F. U., Speich, S. & Biastoch, A. Cold vs. warm water route—sources for the upper limb of the Atlantic Meridional Overturning Circulation revisited in a high-resolution ocean model. *Ocean Sci.* **15**, 489–512 (2019).
66. Biastoch, A., Böning, C. W. & Lutjeharms, J. R. E. Agulhas leakage dynamics affects decadal variability in Atlantic overturning circulation. *Nature* **456**, 489–492 (2008).
67. Bower, A. et al. Lagrangian views of the pathways of the Atlantic Meridional Overturning Circulation. *J. Geophys. Res. Oceans* **124**, 5313–5335 (2019).
68. Gordon, A. L., Weiss, R. F., Smethie, W. M. & Warner, M. J. Thermocline and intermediate water communication between the south Atlantic and Indian oceans. *J. Geophys. Res.* **97**, 7223 (1992).
69. Gordon, A. L. Interocean exchange of thermocline water. *J. Geophys. Res.* **91**, 5037 (1986).
70. Rennell, J. *An investigation of the currents of the Atlantic Ocean: and of those which prevail between the Indian Ocean and the Atlantic*. vol. (OCoLC) 757616581 (Published for Lady Rodd by J.G. & F. Rivington, 1832).
71. Rousselet, L., Cessi, P. & Forget, G. Routes of the upper branch of the Atlantic Meridional Overturning Circulation according to an Ocean State Estimate. *Geophys. Res. Lett.* **47**, e2020GL08913 (2020).
72. Georgi, D. T. Circulation of bottom waters in the southwestern South Atlantic. *Deep Sea Res. Part A* **28**, 959–979 (1981).
73. Coles, V. J., McCartney, M. S., Olson, D. B. & Smethie, W. M. Changes in Antarctic Bottom Water properties in the western South Atlantic in the late 1980s. *J. Geophys. Res.* **101**, 8957–8970 (1996).
74. Valla, D., Piola, A. R., Meinen, C. S. & Campos, E. Abyssal transport variations in the Southwest South Atlantic: first insights from a long-term observation array at 34.5°S. *Geophys. Res. Lett.* **46**, 6699–6705 (2019).
75. Meinen, C. S., Perez, R. C., Dong, S., Piola, A. R. & Campos, E. Observed Ocean Bottom Temperature Variability at Four Sites in the Northwestern Argentine Basin: Evidence of Decadal Deep/Abyssal Warming Amidst Hourly to Interannual Variability During 2009–2019. *Geophys. Res. Lett.* **47**, e2020GL08909 (2020).
76. Campos, E. J. D. et al. Warming Trend in Antarctic Bottom Water in the Vema Channel in the South Atlantic. *Geophys. Res. Lett.* **48**, e2021GL094709 (2021).

77. Arhan, M., Mercier, H. & Park, Y.-H. On the deep water circulation of the eastern South Atlantic Ocean. *Deep Sea Res. Part I* **50**, 889–916 (2003).
78. van Sebille, E., Johns, W. E. & Beal, L. M. Does the vorticity flux from Agulhas rings control the zonal pathway of NADW across the South Atlantic? *J. Geophys. Res.* **117**, C05037 (2012).
79. Xu, X., Chassignet, E. P., Dong, S. & Baringer, M. O. Transport structure of the South Atlantic Ocean derived from a high-resolution numerical model and observations. *Front. Mar. Sci.* **9**, 811398 (2022).
80. Stramma, L. & England, M. On the water masses and mean circulation of the South Atlantic Ocean. *J. Geophys. Res.* **104**, 20863–20883 (1999).
81. Biastoch, A., Böning, C. W., Schwarzkopf, F. U. & Lutjeharms, J. R. E. Increase in Agulhas leakage due to poleward shift of Southern Hemisphere westerlies. *Nature* **462**, 495–498 (2009).
82. Schmid, C. & Garzoli, S. L. New observations of the spreading and variability of the Antarctic Intermediate Water in the Atlantic. *J. Mar. Res.* **67**, 815–843 (2009).
83. Schmid, C. Mean vertical and horizontal structure of the subtropical circulation in the South Atlantic from three-dimensional observed velocity fields. *Deep Sea Res. Part I* **91**, 50–71 (2014).
84. Kersalé, M. et al. Moored observations of mesoscale features in the Cape Basin: characteristics and local impacts on water mass distributions. *Ocean Sci.* **14**, 923–945 (2018).
85. Kersalé, M. et al. Shallow and Deep Eastern Boundary Currents in the South Atlantic at 34.5°S: mean structure and variability. *J. Geophys. Res. Oceans* **124**, 1634–1659 (2019).
86. de Vries, P. The Atlantic freshwater budget as a diagnostic for the existence of a stable shut down of the meridional overturning circulation. *Geophys. Res. Lett.* **32**, L09606 (2005).
87. Dijkstra, H. A. Characterization of the multiple equilibria regime in a global ocean model. *Tellus A* **59**, 695–705 (2007).
88. Huisman, S. E., den Toom, M., Dijkstra, H. A. & Drijfhout, S. An indicator of the multiple equilibria regime of the Atlantic Meridional Overturning Circulation. *J. Phys. Oceanogr.* **40**, 551–567 (2010).
89. Cimatoribus, A. A., Drijfhout, S. S., den Toom, M. & Dijkstra, H. A. Sensitivity of the Atlantic meridional overturning circulation to South Atlantic freshwater anomalies. *Clim. Dyn.* **39**, 2291–2306 (2012).
90. Drijfhout, S. S., Weber, S. L. & van der Swaluw, E. The stability of the MOC as diagnosed from model projections for pre-industrial, present and future climates. *Clim. Dyn.* **37**, 1575–1586 (2011).
91. Weijer, W. et al. Stability of the Atlantic Meridional Overturning Circulation: a review and synthesis. *J. Geophys. Res. Oceans* **124**, 5336–5375 (2019).
92. Cunningham, S. A. et al. Temporal variability of the Atlantic Meridional Overturning Circulation at 26.5°N. *Science* **317**, 935–938 (2007).
93. Send, U., Lankhorst, M. & Kanzow, T. Observation of decadal change in the Atlantic meridional overturning circulation using 10 years of continuous transport data. *Geophys. Res. Lett.* **38**, L24606 (2011).
94. Smeed, D. A. et al. The North Atlantic Ocean is in a state of reduced overturning. *Geophys. Res. Lett.* **45**, 1527–1533 (2018).
95. Lozier, M. S. et al. A sea change in our view of overturning in the subpolar North Atlantic. *Science* **363**, 516–521 (2019).
96. McCarthy, G. D. et al. Sustainable observations of the AMOC: methodology and technology. *Rev. Geophys.* **58**, e2019RG000654 (2020).
97. Kersalé, M. et al. Highly variable upper and abyssal overturning cells in the South Atlantic. *Sci. Adv.* **6**, eaba7573 (2020).
98. Herrford, J. et al. Seasonal variability of the Atlantic Meridional Overturning Circulation at 11° S inferred from bottom pressure measurements. *Ocean Sci.* **17**, 265–284 (2021).
99. Speich, S., Garzoli, S., Piola, A., & SAMOC community. in *Proc. OceanObs'09: Sustained Ocean Observations and Information for Society (Annex), Venice, Italy*, 21–25 September 2009 (eds. Hall, J., Harrison, D. E., & Stammer, D.) (ESA Publication WPP-306, 2010).
100. Meinen, C. S. et al. Temporal variability of the meridional overturning circulation at 34.5°S: results from two pilot boundary arrays in the South Atlantic. *J. Geophys. Res. Oceans* **118**, 6461–6478 (2013).
101. Ansorge, I. J. et al. Basin-wide Oceanographic array bridges the South Atlantic. *Eos Trans. AGU* **95**, 53–54 (2014).
102. Xu, X., Chassignet, E. P., Firing, Y. L. & Donohue, K. Antarctic circumpolar current transport through Drake Passage: what can we learn from comparing high-resolution model results to observations? *J. Geophys. Res. Oceans* **125**, e2020JC016365 (2020).
103. Weijer, W., Cheng, W., Garuba, O. A., Hu, A. & Nadiga, B. T. CMIP6 models predict significant 21st century decline of the Atlantic Meridional Overturning Circulation. *Geophys. Res. Lett.* **47**, e2019GL086075 (2020).
104. Biastoch, A. et al. Regional imprints of changes in the Atlantic Meridional Overturning Circulation in the eddy-rich ocean model VIKING20X. *Ocean Sci.* **17**, 1177–1211 (2021).
105. Wüst, G. & Defant, A. Schichtung und Zirkulation des Atlantischen Ozeans. In: *Wissenschaftliche Ergebnisse der Deutschen Atlantischen Expedition auf dem Forschungs- und Vermessungsschiff 'Meteor' 1925–1927*. Vol. 6, Atlas, 103 plates, Beilagen I-CIII (Walter de Gruyter & Co Berlin, 1936).
106. Defant, A. Quantitative Untersuchungen zur Statik und Dynamik des Atlantischen Ozeans. Die absolute Topographie des physikalischen Meeresniveaus und der Druckflächen, sowie die Wasserbewegungen im Atlantischen Ozean. In: *Wissenschaftliche Ergebnisse der Deutschen Atlantischen Expedition auf dem Forschungs- und Vermessungsschiff 'Meteor' 1925–1927*. Vol. 6 (2,5) 191–160 (Walter de Gruyter & Co Berlin, 1941).
107. Wüst, G. Stromgeschwindigkeiten und Strommengen in den Tiefen des Atlantischen Ozeans unter besonderer Berücksichtigung des Tiefen- und Bodenwassers. In: *Wissenschaftliche Ergebnisse der Deutschen Atlantischen Expedition auf dem Forschungs- und Vermessungsschiff 'Meteor' 1925–1927*. Vol. (2,6), p. 180 (Walter de Gruyter & Co Berlin, 1957).
108. Fuglister, F. C. *Atlantic Ocean atlas of temperature and salinity profiles and data from the International Geophysical Year of 1957–1958*. (Woods Hole Oceanographic Institution, 1960).
109. Reid, J. L. On the total geostrophic circulation of the South Atlantic Ocean: flow patterns, tracers, and transports. *Prog. Oceanogr.* **23**, 149–244 (1989).
110. Sloyan, B. M. et al. The Global Ocean Ship-Based Hydrographic Investigations Program (GO-SHIP): A Platform for Integrated Multidisciplinary Ocean Science. *Front. Mar. Sci.* **6**, 445 (2019).
111. Jayne, S. et al. The Argo Program: present and future. *Oceanography* **30**, 18–28 (2017).
112. Roemmich, D. et al. On the Future of Argo: a global, full-depth, multi-disciplinary array. *Front. Mar. Sci.* **6**, 439 (2019).
113. Chidichimo, M. P. et al. Brazil Current Volume Transport Variability during 2009–2015 from a long-term moored array at 34.5°S. *J. Geophys. Res. Oceans* **126**, e2020JC017146 (2021).
114. Valla, D., Piola, A. R., Meinen, C. S. & Campos, E. Strong mixing and recirculation in the Northwestern Argentine Basin. *J. Geophys. Res. Oceans* **123**, 4624–4648 (2018).
115. Tuchen, F. P., Brandt, P., Lübbecke, J. F. & Hummels, R. Transports and pathways of the tropical AMOC return flow from Argo data and shipboard velocity measurements. *J. Geophys. Res. Oceans* **127**, e2021JC018115 (2022).
116. Drouin, K. L., Lozier, M. S. & Johns, W. E. Variability and trends of the South Atlantic Subtropical Gyre. *J. Geophys. Res. Oceans* **126**, e2020JC016405 (2021).
117. Reid, J. L. On the total geostrophic circulation of the North Atlantic Ocean: flow patterns, tracers, and transports. *Prog. Oceanogr.* **33**, 1–92 (1994).
118. Schmitz, W. J. *On the world ocean circulation. Volume I, Some global features/ North Atlantic circulation*. (Woods Hole Oceanographic Institution, 1996).
119. Speich, S., Blanke, B. & Madec, G. Warm and cold water routes of an O.G.C.M. thermohaline conveyor belt. *Geophys. Res. Lett.* **28**, 311–314 (2001).
120. Weijer, W., de Ruijter, W. P. M., Dijkstra, H. A. & van Leeuwen, P. J. Impact of interbasin exchange on the Atlantic Overturning Circulation. *J. Phys. Oceanogr.* **29**, 2266–2284 (1999).
121. Steinfeldt, R. & Rhein, M. Spreading velocities and dilution of North Atlantic Deep Water in the tropical Atlantic based on CFC time series. *J. Geophys. Res.* **109**, C03046 (2004).
122. Hummels, R. et al. Interannual to decadal changes in the western boundary circulation in the Atlantic at 11°S. *Geophys. Res. Lett.* **42**, 7615–7622 (2015).
123. Schott, F. A. et al. The Shallow and Deep Western Boundary Circulation of the South Atlantic at 5°–11°S. *J. Phys. Oceanogr.* **35**, 2031–2053 (2005).
124. Zhang, D., Msadek, R., McPhaden, M. J. & Delworth, T. Multidecadal variability of the North Brazil Current and its connection to the Atlantic meridional overturning circulation. *J. Geophys. Res.* **116**, C04012 (2011).
125. Rühs, S., Getzlaff, K., Durgadoo, J. V., Biastoch, A. & Böning, C. W. On the suitability of North Brazil Current transport estimates for monitoring basin-scale AMOC changes. *Geophys. Res. Lett.* **42**, 8072–8080 (2015).
126. Hernández-Guerra, A. et al. The upper, deep, abyssal and overturning circulation in the Atlantic Ocean at 30°S in 2003 and 2011. *Prog. Oceanogr.* **176**, 102136 (2019).
127. Sato, O. T. & Polito, P. S. Observation of South Atlantic subtropical mode waters with Argo profiling float data. *J. Geophys. Res. Oceans* **119**, 2860–2881 (2014).
128. Chen, Y., Speich, S. & Laxenaire, R. Formation and transport of the South Atlantic subtropical mode water in Eddy-Permitting observations. *J. Geophys. Res. Oceans* **127**, e2021JC017767 (2022).
129. Piola, A. R. & Gordon, A. L. Intermediate waters in the southwest South Atlantic. *Deep Sea Res. Part A* **36**, 1–16 (1989).
130. Suga, T. & Talley, L. D. Antarctic Intermediate Water circulation in the tropical and subtropical South Atlantic. *J. Geophys. Res.* **100**, 13441 (1995).
131. Rusciano, E., Speich, S. & Ollitrault, M. Interocean exchanges and the spreading of Antarctic Intermediate Water south of Africa. *J. Geophys. Res.* **117**, C10010 (2012).
132. Gordon, A. L., Lutjeharms, J. R. E. & Gründlingh, M. L. Stratification and circulation at the Agulhas Retroflection. *Deep Sea Res. Part A* **34**, 565–599 (1987).

133. Burke, A. et al. The glacial mid-depth radiocarbon bulge and its implications for the overturning circulation: Glacial Radiocarbon and Circulation. *Paleoceanography* **30**, 1021–1039 (2015).
134. Chang, P. et al. Oceanic link between abrupt changes in the North Atlantic Ocean and the African monsoon. *Nat. Geosci.* **1**, 444–448 (2008).
135. Dima, M., Lohmann, G., Ionita, M., Knorr, G. & Scholz, P. AMOC modes linked with distinct North Atlantic deep water formation sites. *Clim. Dyn.* **59**, 837–849 (2022).
136. Zhu, C. & Liu, Z. Weakening Atlantic overturning circulation causes South Atlantic salinity pile-up. *Nat. Clim. Change* **10**, 998–1003 (2020).
137. Kolodziejczyk, N., Reverdin, G., Gaillard, F. & Lazar, A. Low-frequency thermohaline variability in the Subtropical South Atlantic pycnocline during 2002–2013. *Geophys. Res. Lett.* **41**, 6468–6475 (2014).
138. Cheng, L. et al. Upper Ocean temperatures hit record high in 2020. *Adv. Atmos. Sci.* **38**, 523–530 (2021).
139. Johnson, G. C. & Lyman, J. M. Warming trends increasingly dominate global ocean. *Nat. Clim. Change* **10**, 757–761 (2020).
140. Risaro, D. B., Chidichimo, M. P. & Piola, A. R. Interannual variability and trends of sea surface temperature around Southern South America. *Front. Mar. Sci.* **9**, 829144 (2022).
141. Durack, P. J., Wijffels, S. E. & Matear, R. J. Ocean salinities reveal strong global water cycle intensification during 1950 to 2000. *Science* **336**, 455–458 (2012).
142. Aubone, N., Palma, E. D. & Piola, A. R. The surface salinity maximum of the South Atlantic. *Prog. Oceanogr.* **191**, 102499 (2021).
143. Gould, W. J. & Cunningham, S. A. Global-scale patterns of observed sea surface salinity intensified since the 1870s. *Commun. Earth Environ.* **2**, 76 (2021).
144. Arbic, B. K. & Brechner Owens, W. Climatic warming of Atlantic intermediate waters. *J. Clim.* **14**, 4091–4108 (2001).
145. McCarthy, G., McDonagh, E. & King, B. Decadal variability of thermocline and intermediate waters at 24°S in the South Atlantic. *J. Phys. Oceanogr.* **41**, 157–165 (2011).
146. Häkkinen, S., Rhines, P. B. & Worthen, D. L. Heat content variability in the North Atlantic Ocean in ocean reanalyses. *Geophys. Res. Lett.* **42**, 2901–2909 (2015).
147. Desbruyères, D., McDonagh, E. L., King, B. A. & Thierry, V. Global and full-depth Ocean temperature trends during the early twenty-first century from Argo and repeat hydrography. *J. Clim.* **30**, 1985–1997 (2017).
148. Kolodziejczyk, N., Llovel, W. & Portela, E. Interannual variability of upper Ocean water masses as inferred from Argo array. *J. Geophys. Res. Oceans* **124**, 6067–6085 (2019).
149. Bernardo, P. S. & Sato, O. T. Volumetric characterization of the South Atlantic subtropical mode water types. *Geophys. Res. Lett.* **47**, e2019GL086653 (2020).
150. Cheng, L. et al. Improved estimates of changes in Upper Ocean salinity and the hydrological cycle. *J. Clim.* **33**, 10357–10381 (2020).
151. Giglio, D. & Johnson, G. C. Middepth decadal warming and freshening in the South Atlantic. *J. Geophys. Res. Oceans* **122**, 973–979 (2017).
152. Changing Ocean, Marine Ecosystems, and Dependent Communities. in *The Ocean and Cryosphere in a Changing Climate: Special Report of the Intergovernmental Panel on Climate Change* (ed. Intergovernmental Panel on Climate Change (IPCC)) 447–588 (Cambridge University Press, 2022).
153. McCarthy, G. et al. Observed interannual variability of the Atlantic meridional overturning circulation at 26.5°N. *Geophys. Res. Lett.* **39**, L19609 (2012).
154. Xu, X., Chassignet, E. P., Johns, W. E., Schmitz, W. J. & Metzger, E. J. Intraseasonal to interannual variability of the Atlantic meridional overturning circulation from eddy-resolving simulations and observations. *J. Geophys. Res. Oceans* **119**, 5140–5159 (2014).
155. Gastineau, G., Mignot, J., Arzel, O. & Huck, T. North Atlantic Ocean Internal Decadal Variability: Role of the Mean State and Ocean-Atmosphere Coupling. *J. Geophys. Res. Oceans* **123**, 5949–5970 (2018).
156. Park, W. & Latif, M. Multidecadal and multicentennial variability of the meridional overturning circulation. *Geophys. Res. Lett.* **35**, L22703 (2008).
157. Purkey, S. G. & Johnson, G. C. Warming of Global Abyssal and Deep Southern Ocean Waters between the 1990s and 2000s: Contributions to Global Heat and Sea Level Rise Budgets. *J. Clim.* **23**, 6336–6351 (2010).
158. Purkey, S. G. & Johnson, G. C. Antarctic Bottom Water warming and freshening: contributions to Sea Level Rise, Ocean Freshwater Budgets, and Global Heat Gain. *J. Clim.* **26**, 6105–6122 (2013).
159. Johnson, G. C., McTaggart, K. E. & Wanninkhof, R. Antarctic Bottom Water temperature changes in the western South Atlantic from 1989 to 2014. *J. Geophys. Res. Oceans* **119**, 8567–8577 (2014).
160. Desbruyères, D. G., Purkey, S. G., McDonagh, E. L., Johnson, G. C. & King, B. A. Deep and abyssal ocean warming from 35 years of repeat hydrography. *Geophys. Res. Lett.* **43**, 10,356–10,365 (2016).
161. Purkey, S. G. & Johnson, G. C. Global contraction of Antarctic Bottom Water between the 1980s and 2000s. *J. Clim.* **25**, 5830–5844 (2012).
162. Zenk, W. & Morozov, E. Decadal warming of the coldest Antarctic Bottom Water flow through the Vema Channel. *Geophys. Res. Lett.* **34**, L14607 (2007).
163. Johnson, G. C., Cadot, C., Lyman, J. M., McTaggart, K. E. & Steffen, E. L. Antarctic Bottom Water Warming in the Brazil Basin: 1990s through 2020, from WOCE to Deep Argo. *Geophys. Res. Lett.* **47**, e2020GL089191 (2020).
164. Majumder, S., Schmid, C. & Halliwell, G. An observations and model-based analysis of meridional transports in the South Atlantic: transports in the South Atlantic. *J. Geophys. Res. Oceans* **121**, 5622–5638 (2016).
165. Dong, S., Goni, G. & Bringas, F. Temporal variability of the South Atlantic Meridional Overturning Circulation between 20°S and 35°S. *Geophys. Res. Lett.* **42**, 7655–7662 (2015).
166. Bryden, H. L., King, B. A. & McCarthy, G. D. South Atlantic overturning circulation at 24°S. *J. Mar. Res.* **69**, 38–55 (2011).
167. McDonagh, E. L. & King, B. A. Oceanic fluxes in the South Atlantic. *J. Phys. Oceanogr.* **35**, 109–122 (2005).
168. Saunders, P. M. & King, B. A. Bottom currents derived from a shipborne ADCP on WOCE Cruise A11 in the South Atlantic. *J. Phys. Oceanogr.* **25**, 329–347 (1995).
169. de las Heras, M. M. & Schlitzer, R. On the importance of intermediate water flows for the global ocean overturning. *J. Geophys. Res.* **104**, 15515–15536 (1999).
170. Hogg, N. G., Siedler, G. & Zenk, W. Circulation and variability at the Southern Boundary of the Brazil Basin. *J. Phys. Oceanogr.* **29**, 145–157 (1999).
171. Hogg, N. G., Biscaye, P. E., Gardner, W. E. & Schmitz, W. J. Jr On the transport and modification of Antarctic Bottom Water in the vema channel. *J. Mar. Res.* **40**, 231–263 (1982).
172. Zenk, W., Siedler, G., Lenz, B. & Hogg, N. G. Antarctic Bottom Water Flow through the Hunter Channel. *J. Phys. Oceanogr.* **29**, 2785–2801 (1999).
173. Kanzow, T. et al. Observed flow compensation associated with the MOC at 26.5°N in the Atlantic. *Science* **317**, 938–941 (2007).
174. Chidichimo, M. P., Kanzow, T., Cunningham, S. A., Johns, W. E. & Marotzke, J. The contribution of eastern-boundary density variations to the Atlantic meridional overturning circulation at 26.5° N. *Ocean Sci.* **6**, 475–490 (2010).
175. Moat, B. I. et al. Pending recovery in the strength of the meridional overturning circulation at 26° N. *Ocean Sci.* **16**, 863–874 (2020).
176. Gu, S., Liu, Z. & Wu, L. Time Scale Dependence of the Meridional Coherence of the Atlantic Meridional Overturning Circulation. *J. Geophys. Res. Oceans* **125**, e2019JC015838 (2020).
177. Meinen, C. S. et al. Characteristics and causes of Deep Western Boundary Current transport variability at 34.5° S during 2009–2014. *Ocean Sci.* **13**, 175–194 (2017).
178. Kopte, R. et al. The Angola Current: flow and hydrographic characteristics as observed at 11°S. *J. Geophys. Res. Oceans* **122**, 1177–1189 (2017).
179. Imbol Koungue, R. A. & Brandt, P. Impact of Intraseasonal Waves on Angolan Warm and Cold Events. *J. Geophys. Res. Oceans* **126**, e2020JC017088 (2021).
180. Kopte, R., Brandt, P., Claus, M., Greatbatch, R. J. & Dengler, M. Role of Equatorial Basin-Mode Resonance for the Seasonal Variability of the Angola Current at 11°S. *J. Phys. Oceanogr.* **48**, 261–281 (2018).
181. Tchipalanga, P. et al. Eastern boundary circulation and hydrography off Angola: Building Angolan Oceanographic Capacities. *Bull. Am. Meteorol. Soc.* **99**, 1589–1605 (2018).
182. Dong, S., Garzoli, S. & Baringer, M. The Role of Interocean Exchanges on Decadal Variations of the Meridional Heat Transport in the South Atlantic. *J. Phys. Oceanogr.* **41**, 1498–1511 (2011).
183. Volkov, D. et al. Meridional overturning circulation and heat transport in the Atlantic Ocean [in State of the Climate in 2020]. *Bull. Am. Meteorol. Soc.* **102**, s176–s179 (2020).
184. Caínzos, V. et al. Thirty years of GOSHIP and WOCE Data: Atlantic Overturning of mass, heat, and freshwater transport. *Geophys. Res. Lett.* **49**, e2021GL096527 (2022).
185. Ganachaud, A. & Wunsch, C. Large-Scale Ocean heat and freshwater transports during the World Ocean Circulation Experiment. *J. Clim.* **16**, 696–705 (2003).
186. McDonagh, E. L. et al. Continuous estimate of Atlantic Oceanic freshwater Flux at 26.5°N. *J. Clim.* **28**, 8888–8906 (2015).
187. Whitworth, T., Nowlin, W. D. & Worley, S. J. The net transport of the Antarctic Circumpolar Current through Drake Passage. *J. Phys. Oceanogr.* **12**, 960–971 (1982).
188. Whitworth, T. Monitoring the transport of the Antarctic Circumpolar Current at Drake Passage. *J. Phys. Oceanogr.* **13**, 2045–2057 (1983).
189. Cunningham, S. A. Transport and variability of the Antarctic Circumpolar Current in Drake Passage. *J. Geophys. Res.* **108**, 8084 (2003).
190. Koenig, Z., Provost, C., Ferrari, R., Sennéchael, N. & Rio, M.-H. Volume transport of the Antarctic Circumpolar Current: Production and validation of a 20 year long time series obtained from in situ and satellite observations. *J. Geophys. Res. Oceans* **119**, 5407–5433 (2014).

191. Chidichimo, M. P., Donohue, K. A., Watts, D. R. & Tracey, K. L. Baroclinic transport time series of the Antarctic Circumpolar Current Measured in Drake Passage. *J. Phys. Oceanogr.* **44**, 1829–1853 (2014).
192. Donohue, K. A., Tracey, K. L., Watts, D. R., Chidichimo, M. P. & Chereskin, T. K. Mean Antarctic Circumpolar Current transport measured in Drake Passage. *Geophys. Res. Lett.* **43**, 11,760–11,767 (2016).
193. Colin de Verdière, A. & Ollitrault, M. A direct determination of the World Ocean Barotropic Circulation. *J. Phys. Oceanogr.* **46**, 255–273 (2016).
194. Chassignet, E. P., Smith, L. T., Halliwell, G. R. & Bleck, R. North Atlantic Simulations with the Hybrid Coordinate Ocean Model (HYCOM): impact of the vertical coordinate choice, reference pressure, and thermobaricity. *J. Phys. Oceanogr.* **33**, 2504–2526 (2003).
195. Artana, C. et al. Twenty-five years of Mercator ocean reanalysis GLORYS12 at Drake Passage: Velocity assessment and total volume transport. *Adv. Space Res.* **68**, 447–466 (2021).
196. Peña-Molino, B., Rintoul, S. R. & Mazloff, M. R. Barotropic and baroclinic contributions to along-stream and across-stream transport in the Antarctic Circumpolar Current. *J. Geophys. Res. Oceans* **119**, 8011–8028 (2014).
197. Meredith, M. P. et al. Sustained monitoring of the Southern Ocean at Drake Passage: past achievements and future priorities. *Rev. Geophys.* **49**, RG4005 (2011).
198. Firing, Y. L., Chereskin, T. K. & Mazloff, M. R. Vertical structure and transport of the Antarctic Circumpolar Current in Drake Passage from direct velocity observations. *J. Geophys. Res.* **116**, C08015 (2011).
199. Durgadoo, J. V., Loveday, B. R., Reason, C. J. C., Penven, P. & Biastoch, A. Agulhas leakage predominantly responds to the Southern Hemisphere Westerlies. *J. Phys. Oceanogr.* **43**, 2113–2131 (2013).
200. Swart, N. C., Fyfe, J. C., Gillett, N. & Marshall, G. J. Comparing trends in the Southern Annular Mode and Surface Westerly Jet. *J. Clim.* **28**, 8840–8859 (2015).
201. Hallberg, R. & Gnanadesikan, A. The Role of Eddies in Determining the Structure and Response of the Wind-Driven Southern Hemisphere Overturning: Results from the Modeling Eddies in the Southern Ocean (MESO) Project. *J. Phys. Oceanogr.* **36**, 2232–2252 (2006).
202. Hogg, A. Mc. C. et al. Recent trends in the Southern Ocean eddy field. *J. Geophys. Res. Oceans* **120**, 257–267 (2015).
203. Marshall, D. P., Ambaum, M. H. P., Maddison, J. R., Munday, D. R. & Novak, L. Eddy saturation and frictional control of the Antarctic Circumpolar Current: Eddy Saturation of the ACC. *Geophys. Res. Lett.* **44**, 286–292 (2017).
204. Bryden, H. L. Poleward heat flux and conversion of available potential energy in Drake Passage. *J. Mar. Res.* **37**, 1–22 (1979).
205. Johnson, G. C. & Bryden, H. L. On the size of the Antarctic Circumpolar Current. *Deep Sea Research Part A* **36**, 39–53 (1989).
206. Chereskin, T., Donohue, K. & Watts, R. cDrake: dynamics and transport of the Antarctic Circumpolar Current in Drake Passage. *Oceanography* **25**, 134–135 (2012).
207. Watts, D. R., Tracey, K. L., Donohue, K. A. & Chereskin, T. K. Estimates of Eddy Heat Flux Crossing the Antarctic Circumpolar Current from Observations in Drake Passage. *J. Phys. Oceanogr.* **46**, 2103–2122 (2016).
208. Lenn, Y.-D., Chereskin, T. K., Sprintall, J. & McClean, J. L. Near-surface Eddy Heat and Momentum Fluxes in the Antarctic Circumpolar Current in Drake Passage. *J. Phys. Oceanogr.* **41**, 1385–1407 (2011).
209. Gutierrez-Villanueva, M. O., Chereskin, T. K. & Sprintall, J. Upper-Ocean Eddy Heat Flux across the Antarctic Circumpolar Current in Drake Passage from Observations: Time-Mean and Seasonal Variability. *J. Phys. Oceanogr.* **50**, 2507–2527 (2020).
210. Cheng, Y., Putrasahan, D., Beal, L. & Kirtman, B. Quantifying Agulhas Leakage in a high-resolution climate model. *J. Clim.* **29**, 6881–6892 (2016).
211. Boebel, O. et al. The Cape Cauldron: a regime of turbulent inter-ocean exchange. *Deep Sea Res. Part II* **50**, 57–86 (2003).
212. Dencausse, G., Arhan, M. & Speich, S. Is there a continuous Subtropical Front south of Africa? *J. Geophys. Res.* **116**, C02027 (2011).
213. Capuano, T. A., Speich, S., Carton, X. & Blanke, B. Mesoscale and Submesoscale processes in the Southeast Atlantic and their impact on the regional thermohaline structure. *J. Geophys. Res. Oceans* **123**, 1937–1961 (2018).
214. Capuano, T. A., Speich, S., Carton, X. & Laxenaire, R. Indo-Atlantic Exchange, Mesoscale Dynamics, and Antarctic Intermediate Water. *J. Geophys. Res. Oceans* **123**, 3286–3306 (2018).
215. Daher, H., Beal, L. M. & Schwarzkopf, F. U. A new improved estimation of Agulhas Leakage using observations and simulations of Lagrangian Floats and Drifters. *J. Geophys. Res. Oceans* **125**, e2019JC015753 (2020).
216. Laxenaire, R., Speich, S. & Stegner, A. Evolution of the thermohaline structure of One Agulhas ring reconstructed from Satellite Altimetry and Argo Floats. *J. Geophys. Res. Oceans* **124**, 8969–9003 (2019).
217. van Ballegooyen, R. C., Gründlingh, M. L. & Lutjeharms, J. R. E. Eddy fluxes of heat and salt from the southwest Indian Ocean into the southeast Atlantic Ocean: a case study. *J. Geophys. Res.* **99**, 14053 (1994).
218. Arhan, M., Mercier, H. & Lutjeharms, J. R. E. The disparate evolution of three Agulhas rings in the South Atlantic Ocean. *J. Geophys. Res.* **104**, 20987–21005 (1999).
219. Arhan, M. et al. Anticyclonic and cyclonic eddies of subtropical origin in the subantarctic zone south of Africa. *J. Geophys. Res.* **116**, 2011JC007140 (2011).
220. Garzoli, S. L. et al. Three Agulhas rings observed during the Benguela Current Experiment. *J. Geophys. Res.* **104**, 20971–20985 (1999).
221. Beron-Vera, F. J., Wang, Y., Olascoaga, M. J., Goni, G. J. & Haller, G. Objective detection of Oceanic Eddies and the Agulhas Leakage. *J. Phys. Oceanogr.* **43**, 1426–1438 (2013).
222. Laxenaire, R. et al. Anticyclonic Eddies Connecting the Western Boundaries of Indian and Atlantic Oceans. *J. Geophys. Res. Oceans* **123**, 7651–7677 (2018).
223. Doglioli, A. M., Veneziani, M., Blanke, B., Speich, S. & Griffa, A. A Lagrangian analysis of the Indian-Atlantic interocean exchange in a regional model. *Geophys. Res. Lett.* **33**, L14611 (2006).
224. Loveday, B. R., Penven, P. & Reason, C. J. C. Southern Annular Mode and westerly-wind-driven changes in Indian-Atlantic exchange mechanisms. *Geophys. Res. Lett.* **42**, 4912–4921 (2015).
225. Laxenaire, R., Speich, S. & Stegner, A. Agulhas ring heat content and transport in the South Atlantic estimated by combining Satellite Altimetry and Argo Profiling Floats Data. *J. Geophys. Res. Oceans* **125**, e2019JC015511 (2020).
226. Nencioli, F., Dall'Olmo, G. & Quartly, G. D. Agulhas ring transport efficiency from combined Satellite Altimetry and Argo Profiles. *J. Geophys. Res. Oceans* **123**, 5874–5888 (2018).
227. Beal, L. M. et al. On the role of the Agulhas system in ocean circulation and climate. *Nature* **472**, 429–436 (2011).
228. Loveday, B. R., Durgadoo, J. V., Reason, C. J. C., Biastoch, A. & Penven, P. Decoupling of the Agulhas Leakage from the Agulhas Current. *J. Phys. Oceanogr.* **44**, 1776–1797 (2014).
229. Elipot, S. & Beal, L. M. Characteristics, energetics, and origins of Agulhas Current Meanders and their limited influence on ring shedding. *J. Phys. Oceanogr.* **45**, 2294–2314 (2015).
230. Gladyshev, S., Arhan, M., Sokov, A. & Speich, S. A hydrographic section from South Africa to the southern limit of the Antarctic Circumpolar Current at the Greenwich meridian. *Deep Sea Res. Part I* **55**, 1284–1303 (2008).
231. Thorpe, R. B., Gregory, J. M., Johns, T. C., Wood, R. A. & Mitchell, J. F. B. Mechanisms determining the Atlantic thermohaline circulation response to greenhouse gas forcing in a non-flux-adjusted coupled climate model. *J. Clim.* **14**, 3102–3116 (2001).
232. Smith, R. S. & Gregory, J. M. A study of the sensitivity of ocean overturning circulation and climate to freshwater input in different regions of the North Atlantic. *Geophys. Res. Lett.* **36**, L15701 (2009).
233. Dong, S., Garzoli, S., Baringer, M., Meinen, C. & Goni, G. Interannual variations in the Atlantic meridional overturning circulation and its relationship with the net northward heat transport in the South Atlantic. *Geophys. Res. Lett.* **36**, L20606 (2009).
234. Dong, S., Baringer, M., Goni, G. & Garzoli, S. Importance of the assimilation of Argo float measurements on the Meridional Overturning Circulation in the South Atlantic. *Geophys. Res. Lett.* **38**, L18603 (2011).
235. Böning, C. W., Dieterich, C., Barnier, B. & Jia, Y. Seasonal cycle of meridional heat transport in the subtropical North Atlantic: a model intercomparison in relation to observations near 25°N. *Prog. Oceanogr.* **48**, 231–253 (2001).
236. Jayne, S. R. & Marotzke, J. The dynamics of ocean heat transport variability. *Rev. Geophys.* **39**, 385–411 (2001).
237. Baringer, M. O. et al. Meridional overturning circulation and heat transport observations in the Atlantic Ocean [in State of the Climate in 2012]. *Bull. Am. Meteorol. Soc.* **94**, s65–s68 (2013).
238. Msadek, R. et al. The Atlantic Meridional Heat Transport at 26.5°N and its relationship with the MOC in the RAPID array and the GFDL and NCAR coupled models. *J. Clim.* **26**, 4335–4356 (2013).
239. Dong, S., Baringer, M. O., Goni, G. J., Meinen, C. S. & Garzoli, S. L. Seasonal variations in the South Atlantic Meridional Overturning Circulation from observations and numerical models: SAMOC Seasonal Variations. *Geophys. Res. Lett.* **41**, 4611–4618 (2014).
240. Cheng, W. et al. Can the salt-advection feedback be detected in internal variability of the Atlantic Meridional Overturning Circulation? *J. Clim.* **31**, 6649–6667 (2018).
241. Mecking, J. V., Drijfhout, S. S., Jackson, L. C. & Andrews, M. B. The effect of model bias on Atlantic freshwater transport and implications for AMOC bi-stability. *Tellus A* **69**, 1299910 (2017).
242. Weaver, A. J. et al. Stability of the Atlantic meridional overturning circulation: a model intercomparison. *Geophys. Res. Lett.* **39**, 2012GL053763 (2012).
243. Dengler, M. et al. Break-up of the Atlantic deep western boundary current into eddies at 8° S. *Nature* **432**, 1018–1020 (2004).

244. Gronholz, A. et al. Interannual variability of the South Atlantic Ocean heat content in a high-resolution versus a low-resolution general circulation model. *Geophys. Res. Lett.* **47**, e2020GL089908 (2020).
245. Framing and Context of the Report. in *The Ocean and Cryosphere in a Changing Climate: Special Report of the Intergovernmental Panel on Climate Change* (ed. Intergovernmental Panel on Climate Change (IPCC)) 73–130 (Cambridge University Press, 2022).
246. Roemmich, D. & Gilson, J. The 2004–2008 mean and annual cycle of temperature, salinity, and steric height in the global ocean from the Argo Program. *Prog. Oceanogr.* **82**, 81–100 (2009).
247. Perez, R. C. et al. Measuring the Atlantic Meridional Overturning Circulation. *Mar. Technol. Soc. J.* **49**, 167–177 (2015).
248. Baringer, M. O. & Garzoli, S. L. Meridional heat transport determined with expendable bathythermographs—Part I: Error estimates from model and hydrographic data. *Deep Sea Res. Part I* **54**, 1390–1401 (2007).
249. Ganachaud, A. Large-scale mass transports, water mass formation, and diffusivities estimated from World Ocean Circulation Experiment (WOCE) hydrographic data. *J. Geophys. Res.* **108**, 3213 (2003).
250. Talley, L. D., Reid, J. L. & Robbins, P. E. Data-based Meridional Overturning Streamfunctions for the Global Ocean. *J. Clim.* **16**, 3213–3226 (2003).
251. Meinen, C. S., Piola, A. R., Perez, R. C. & Garzoli, S. L. Deep Western Boundary Current transport variability in the South Atlantic: preliminary results from a pilot array at 34.5° S. *Ocean Sci.* **8**, 1041–1054 (2012).
252. Lopez, H., Goni, G. & Dong, S. A reconstructed South Atlantic Meridional Overturning Circulation time series since 1870. *Geophys. Res. Lett.* **44**, 3309–3318 (2017).
253. Nowlin, W. D., Whitworth, T. & Pillsbury, R. D. Structure and transport of the Antarctic Circumpolar Current at Drake Passage from Short-Term Measurements. *J. Phys. Oceanogr.* **7**, 788–802 (1977).
254. Sprintall, J., Chereskin, T. & Sweeney, C. High-resolution Underway Upper Ocean and Surface Atmospheric Observations in Drake Passage: synergistic measurements for climate science. *Oceanography* **25**, 70–81 (2012).
255. Ansorge, I. J. et al. Monitoring the oceanic flow between Africa and Antarctica: report of the first GoodHope cruise. *S. Afr. J. Sci.* **101**, 29–35 (2005).
256. Speich, S. & Arhan, M. GOODHOPE/Southern Ocean: a study and monitoring of the Indo-Atlantic connections (An international cooperative project. A process study and a contribution to CLIVAR—Southern Ocean). *Mercator Newslett.* **27**, 29–41 (2007).
257. Byrne, D. A. & McClean, J. L. Sea level anomaly signals in the Agulhas Current region. *Geophys. Res. Lett.* **35**, L13601 (2008).
258. Garzoli, S. L. & Gordon, A. L. Origins and variability of the Benguela Current. *J. Geophys. Res.* **101**, 897–906 (1996).
259. Garzoli, S. L., Gordon, A. L., Kamenkovich, V., Pillsbury, D. & Duncombe-Rae, C. Variability and sources of the southeastern Atlantic circulation. *J. Mar. Res.* **54**, 1039–1071 (1996).
260. Bryden, H. L., Beal, L. M. & Duncan, L. M. Structure and transport of the Agulhas Current and its temporal variability. *J. Oceanogr.* **61**, 479–492 (2005).
261. Beal, L. M., Elipot, S., Houk, A. & Leber, G. M. Capturing the transport variability of a Western Boundary Jet: Results from the Agulhas Current Time-Series Experiment (ACT). *J. Phys. Oceanogr.* **45**, 1302–1324 (2015).
262. Morris, T. et al. The importance of monitoring the Greater Agulhas Current and its inter-ocean exchanges using large mooring arrays. *S. Afr. J. Sci.* **113**, 1–7 (2017).

Acknowledgements

M.P.C. acknowledges support by the European Union's Horizon 2020 Research and Innovation Programme under grant agreement no. 818123 (iAtlantic), prior added support from the Inter-American Institute for Global Change Research (IAI) grant CRN3070 (U.S. National Science Foundation grant GEO-1128040), and the additional support from Consejo Nacional de Investigaciones Científicas y Técnicas (CONICET) and Servicio de Hidrografía Naval. R.C.P., S.D., and C.S. were supported via the NOAA's Global Ocean Monitoring and Observing program (FundRef number 100007298) under the Southwest Atlantic Meridional Overturning Circulation (SAM) project, the State of Climate for the meridional heat transport project, the AOML XBT project, the Argo project; via the Climate Program Office (CPO), Climate Observations and Monitoring (COM), and Climate Variability and Predictability (CVP) programs under NOFO NOAA-OAR-CPO-2021-2006389; and with additional support from the NOAA Atlantic Oceanographic and Meteorological Laboratory. S.S. acknowledges support by the European Union's Horizon 2020 research and innovation program under grant agreements no. 633211 (AtlantOS) and no. 817578 (TRIATLAS), the French TOEddies CNES-TOSCA and the 11-ANR-56-004 SAMOC research grants, the LEFE–GMMC/Coriolis program and, for data analyses, on the mesoscale calculation server CICLAD (http://ciclad-web.ipsl.jussieu.fr) of the Institut Pierre Simon Laplace in Paris (France). M.K. acknowledges prior support from the Cooperative Institute for Marine and Atmospheric Studies (CIMAS), a Cooperative Institute of the University of Miami and NOAA (cooperative agreement NA20OAR4320472), and from the NOAA Climate Variability Program (GC16-212) and NASA (80NSSC18K0773). J.S. and T.K.C. were supported by the U.S. National Science Foundation (NSF) Office of Polar Programs Antarctic Division (ANT) through grant ANT-2001646 and the NSF Division of Ocean Sciences (OCE) grant OCE-1755529. J.S. was supported by the NOAA's Global Ocean Monitoring and Observing Program Award NA20OAR4320278. T.L. acknowledges funding and administrative and logistical support from the South African Department of Forestry, Fisheries and the Environment (DFFE), the South African National Research Foundation (NRF; grant number 129229), and the Bayworld Centre for Research and Education (BCRE). O.S. acknowledges the support from the Fundação de Amparo à Pesquisa do Estado de São Paulo (FAPESP), Brazil, under the grant 2017-09659-6; the Brazilian Navy, Petróleo Brasileiro S.A. (PETROBRAS), and the Brazilian Oil Regulatory Agency (ANP) for making the field campaigns possible using the Cooperation Term SIGITEC 2018/00451-6 and 2018/00452-2; and the additional support from the University of São Paulo. R.H. acknowledges support by the European Union's Horizon 2020 research and innovation program under grant agreement no. 817578 (TRIATLAS). We thank the crews of *ARA Puerto Deseado* and *SV Ice Lady Patagonia II* (Argentina), *N.Oc. Alpha Crucis*, *B.Pq. Alpha Delphini*, *N.Oc. Antares*, and the *NHo Cruzeiro do Sul* (Brazil), *R/V Maria S. Merian* (Germany), the *RS Algoa* and *SA Agulhas II* (South Africa) and the *ARSV Laurence M. Gould* (USA) who have supported the research cruises. We also thank the support/technical teams in Miami, São Paulo, Buenos Aires, Paris, Brest, Cape Town, Kiel, and the U.S. Antarctic Support Contractor technicians and cruise volunteers, who have helped collect and/or process the data presented herein. We acknowledge the SAMOC Executive Committee for their support. We thank Chris Meinen and Matthieu Le Hénaff for helpful comments that improved earlier versions of this review, and Bertrand Dano, Gastón Manta, and Xiabiao Xu for providing schematics and figures for the article. We also thank Bertrand Dano for the three-dimensional visualization of the overturning pathways that is available in the supplementary materials. We gratefully acknowledge Regina R. Rodrigues for inspiring the idea of writing a review article focused on the SAMOC initiative. We are grateful for the helpful comments by two anonymous reviewers.

Author contributions

M.P.C. led the writing of the text and coordinated the contributions. M.P.C., R.C.P., S.S., M.K., J.S., and S.D. led individual sections of the text. T.L., O.S., T.K.C., R.H., and C.S. all provided text contributions for individual sections of the text. M.P.C. and all of the coauthors read and provided comments on the entire manuscript. M.P.C., R.C.P., and J.S. edited the text for continuity between sections. M.P.C., R.C.P., M.K., and J.S. produced the display items with data assembled and/or provided by M.P.C., R.C.P., S.S., M.K., S.D., J.S., T.K.C., R.H., and C.S.

Competing interests

The authors declare no competing interests.

Additional information

Supplementary information The online version contains supplementary material available at https://doi.org/10.1038/s43247-022-00644-x.

Correspondence and requests for materials should be addressed to María Paz Chidichimo.

Peer review information *Communications Earth & Environment* thanks Casimir de Lavergne and Corinne Trott for their contribution to the peer review of this work. Primary Handling Editors: Joe Aslin, Heike Langenberg.

Reprints and permission information is available at http://www.nature.com/reprints

Publisher's note Springer Nature remains neutral with regard to jurisdictional claims in published maps and institutional affiliations.